

Architecture and Evolution of the Southern Chotts-Jeffara Basin, Tunisia

Bruna, P. O.; Bertotti, G.; Charton, R. J.G.; Dixon, R.; Nasri, A.

DOI

[10.1029/2023TC008085](https://doi.org/10.1029/2023TC008085)

Publication date

2023

Document Version

Final published version

Published in

Tectonics

Citation (APA)

Bruna, P. O., Bertotti, G., Charton, R. J. G., Dixon, R., & Nasri, A. (2023). Architecture and Evolution of the Southern Chotts-Jeffara Basin, Tunisia. *Tectonics*, 42(12), Article e2023TC008085.
<https://doi.org/10.1029/2023TC008085>

Important note

To cite this publication, please use the final published version (if applicable).
Please check the document version above.

Copyright

Other than for strictly personal use, it is not permitted to download, forward or distribute the text or part of it, without the consent of the author(s) and/or copyright holder(s), unless the work is under an open content license such as Creative Commons.

Takedown policy

Please contact us and provide details if you believe this document breaches copyrights.
We will remove access to the work immediately and investigate your claim.

Key Points:

- Two large scale cross sections across the Southern Chotts-Jeffara basin allowed to interpret multiscale architecture of the basin
- The basin deformation is controlled by the emplacement of anticlines and basin related to successive shortening regimes
- Outcrop observations, seismic-well interpretation and low temperature thermochronology data allow to reconstruct the evolution of the basin

Supporting Information:

Supporting Information may be found in the online version of this article.

Correspondence to:

P.-O. Bruna,
p.b.r.bruna@tudelft.nl

Citation:

Bruna, P.-O., Bertotti, G., Charton, R. J. G., Dixon, R., & Nasri, A. (2023). Architecture and evolution of the Southern Chotts-Jeffara basin, Tunisia. *Tectonics*, 42, e2023TC008085. <https://doi.org/10.1029/2023TC008085>

Received 1 SEP 2023

Accepted 28 NOV 2023



Author Contributions:

Conceptualization: P.-O. Bruna
Data curation: R. J. G. Charton
Formal analysis: P.-O. Bruna, G. Bertotti
Investigation: P.-O. Bruna, G. Bertotti, R. J. G. Charton, R. Dixon
Methodology: P.-O. Bruna, G. Bertotti, R. J. G. Charton
Project Administration: P.-O. Bruna, G. Bertotti
Resources: A. Nasri
Supervision: G. Bertotti
Validation: R. J. G. Charton
Visualization: P.-O. Bruna

© 2023. The Authors.

This is an open access article under the terms of the [Creative Commons Attribution-NonCommercial-NoDerivs License](#), which permits use and distribution in any medium, provided the original work is properly cited, the use is non-commercial and no modifications or adaptations are made.

Architecture and Evolution of the Southern Chotts-Jeffara Basin, Tunisia

P.-O. Bruna^{1,2} , G. Bertotti^{1,2}, R. J. G. Charton^{1,2} , R. Dixon^{2,3}, and A. Nasri⁴

¹Department of Geoscience and Engineering, Delft University of Technology, Delft, The Netherlands, ²North Africa Research Group (NARG), The University of Manchester, Manchester, UK, ³School of Earth and Environmental Sciences, The University of Manchester, Manchester, UK, ⁴Mazarine-Energy Tunisia, Tunis, Tunisia

Abstract Southern Tunisia is known to be less deformed and simpler than its neighboring Atlasic domain to the north. This area is complex and basin evolution in the Southern Chotts-Jeffara (SCJ) basin is debated. In this paper we combined surface and subsurface data with low temperature thermochronology (LTT) to reinvestigate the tectono-sedimentary evolution of the SCJ basin from Permian to Jurassic. We reconstruct the present-day architecture of the SCJ basin along two regional sections. In these sections, we focused mainly on regional thickness variations and on internal reflections interpreted from seismic data. We observe three structural elements: (a) A Paleozoic culmination, oriented E-W, capped by Mid-Upper Triassic deposits; (b) the Tebaga of Medenine (ToM), a culmination also oriented E-W but located ~50 km north of the Paleozoic culmination; and (c) A Triassic culmination in the eastern part of the area, oriented NW-SE. We note the absence of major normal faults along the sections. The LTT data we present are the first published in this area and allow to reconstruct the timing and magnitude of vertical movements. These data prove: (a) exhumation at ~230 Ma of the Permian and Lower Triassic units associated with the onset of the ToM removing locally about 900 m of pre-Cretaceous sediments; and (b) the development of the Triassic culmination ~180 Ma removing 2000 m of pre-Cretaceous sediments in the Jebel Rehach. This study demonstrates that vertical movements in the SCJ basin are controlled by long-wavelength processes developed essentially in shortening regimes.

1. Introduction

Southern Tunisia is an area of great regional interest to constrain the architecture and evolution of sedimentary basins in the central sectors of North Africa. The area includes unique outcrops such as the only exposures of marine Permian sediments in North Africa (Raulin et al., 2011) and references herein) as well as a large amount of subsurface data (seismic and wells). The combination and interpretation of these data provide context for broadly similar sedimentary successions to the west (toward the Algerian border), south (Ghadames and Berkine basins) and east (Libya, where outcrops are more limited, not as well-known and currently less accessible).

In this study, we focus on the formation and deformation of Permian to Jurassic sedimentary successions deposited in the onshore area south of the Chotts ranges. The associated sedimentary basins have various names in the literature and we will adopt the informal term of Southern Chotts-Jeffara (SCJ) basin (e.g., Soua, 2014). This large (ca. 70,000 km²) basin developed following the Variscan unconformity (*sensu lato*), during Tethyan opening and prior to the initial stages of Alpine shortening. In this paper, we address changes in the shape, position and timing of depocentres, location of basin closures and source areas, and we will discuss possible mechanisms driving the SCJ basin evolution.

We first integrate seismic, well and outcrop data from the eastern part of the SCJ basin (inclusive of the Jeffara escarpment and the adjacent Jeffara plain) to reconstruct the architecture of the SCJ Basin along two regional sections, oriented N-S and NE-SW intersecting at a high angle the identified first order structural trends of the area. We then focus on the evolution of the SCJ basin by analyzing and integrating horizontal deformations and absolute vertical movements (both downward and upward). To constrain absolute vertical movements, we have successfully performed Low-Temperature Thermochronology (LTT) on two outcropping samples that provided relevant and robust results. To our knowledge, this is first published LTT data set in the region. Similar to that already documented in Morocco and Mauritania (Bertotti & Gouiza, 2012; Ghorbal et al., 2008; Gouiza et al., 2019), LTT ages and Time-Temperature Modeling (tTM) reveal unexpected vertical movements (burial and exhumation) which could not be directly inferred with other tools.

Writing – original draft: P.-O. Bruna, R. J. G. Charton, R. Dixon
Writing – review & editing: P.-O. Bruna, G. Bertotti, R. J. G. Charton, R. Dixon, A. Nasri

Our new work and results compliment, but also question previous interpretations of the basins evolution and history of uplift and subsidence (Bouaziz et al., 2002; Raulin et al., 2011; Stampfli & Borel, 2002) and we see our work as a constructive contribution to the understanding of this complex region.

2. The Southern Chotts-Jeffara Basin

2.1. The Area of Interest

The area of interest (Figure 1) is mainly located in southern Tunisia between the Atlasic domain in the north and the more stable Saharan domain in the south (Burolet, 1991; Gharbi et al., 2013). The region has been the subject of thorough studies since those of Mathieu (1949) resulting in an extensive and generally accessible high-quality literature database (e.g., Gabtni et al., 2009; Zaafour et al., 2017). Here, we only provide a very brief summary of the regional events leading to the observed Present-day architecture.

2.2. Tectonic Evolution

Variscan shortening in North Africa (Simancas et al., 2005) resulted in a series of exposed (e.g., the Anti-Atlas of Morocco and the Gargaf Arch, Figure 1, (Eschard et al., 2010)) or buried (e.g., the Tibetsi Arch of Libya and the Telemzane Arch, Figure 1), anticlinal structures, generally called “arches,” “highs” or “uplifts.” These arches are in the order of 100s of km long and 10s of km wide and are variably oriented at the regional scale. The area of work includes one of those geological structure buried under the Mesozoic and Cenozoic cover, named the Telemzane Arch ((Acheche et al., 2001; Soua, 2013; Troudi et al., 2018), Figure 1). While various authors have different opinions as to the geometry and age of the structure, it is generally assumed that the Telemzane Arch runs roughly in E-W direction from Algeria to Libya. The detailed analysis and interpretation of the Telemzane Arch falls beyond the scope of this paper.

The lower part of the Carboniferous (Tournaisian) is apparently absent in southern Tunisia (as it is in Morocco, Algeria and Libya (Lubeseder et al., 2010)), this Base Visean unconformity probably marking an important regional phase of Variscan shortening in North Africa. In southern Tunisia, the Visean to Moscovian strata are themselves folded suggesting that Variscan shortening continued at least until the end of the Carboniferous. Thrust-top carbonate platforms developed on these structures testify to their continued growth throughout the Carboniferous (Dixon et al., 2022).

The literature covering the geological history after the important Early Paleozoic/Carboniferous “Variscan” events becomes more controversial. For many authors, Permian times are associated with the onset of the Tethyan rifting phase (Guiraud et al., 2005; Stampfli & Borel, 2002). The occurrence of this rifting in the SCJ basin has been justified by the presence of normal faults described in the subsurface of the NE border of the Jeffara plain and often referred as the “Jeffara Fault System” (Gabtni et al., 2009). This fault system, supposedly oriented NW-SE, is not imaged on seismic data (Raulin et al., 2011).

Work with a more global focus showed that the areas affected by the Tethys rifting are only located in the north of Tunisia (Scotese & Schettino, 2017). Furthermore, there is no Permian oceanic crust in the direct vicinity of the SCJ basin, with the closest occurrence being located ~600–650 km to the NW. The literature also describes gentle folds in the Permian series capped by a second large-scale unconformity, located this time within the Middle Triassic (Raulin et al., 2011).

Triassic to Jurassic times are marked by the opening of the Neo-Tethys Ocean (Chamot-Rooke et al., 2005) propagating from E to W which should have led to the establishment of a narrow strip of oceanic crust, 100s of km to the NE of the investigated area. The area of interest is defined by Raulin et al. (2011) as a proximal margin of the Neo-Tethys Ocean at this time.

Alpine shortening in this part of North Africa began in Late Cretaceous time, following the onset of drifting in the Equatorial and South Atlantic Oceans (Frizon de Lamotte et al., 2011), and persisted until the middle-late Eocene resulting in the incorporation of northern Tunisia and adjacent Algeria and Sicily within the Tell-Riff fold-and-thrust belt system (e.g., Bodin et al., 2010). To the south, in front of the most intensively deformed belt, gentle anticlines, that is, the Chotts Ranges, and associated unconformities have been documented (Saïd et al., 2011).

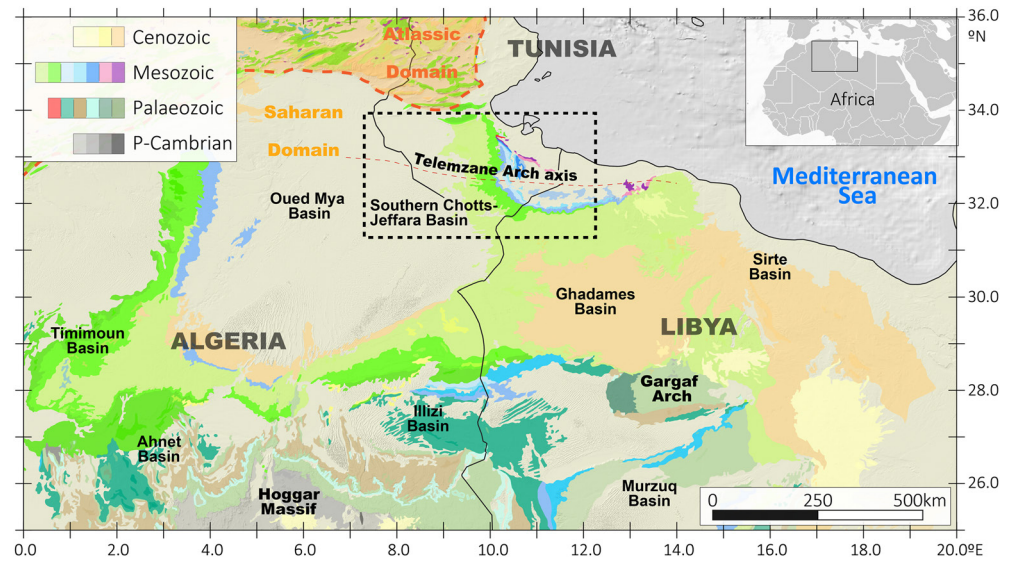


Figure 1. Regional geological map. The map locates the boundary between Atlasic and Saharan domains, the principal sedimentary basins and the exposed or buried reliefs (Arches and Massifs). The area of interest is included into the dashed rectangle. The legend on the top left corner corresponds to the different period of each era.

3. Material and Methods

In this study we propose a new tectonic model for the SCJ area based on: (a) the reconstruction of the present-day regional architecture of the basin using subsurface and surface data and (b) a quantitative analysis of vertical movements recorded in the area of interest using low temperature thermochronology data.

3.1. Surface and Subsurface Data

3.1.1. Seismic and Well Data

To observe the present day regional architecture of the SCJ basin, we have used literature data (2D lines, (Gabtni et al., 2012; Zaafour et al., 2017)), 22 2D seismic lines for a total of 832 km (among which the used ones are synthesized in Table 1) and initial reports (lithological, biostratigraphy and a variety of logs) from 15 boreholes drilled (Table 2) between 1957 and 1987. We are not able to publish original borehole and seismic data because they are confidential. However, we provide in this paper detailed line drawing of our interpretations.

Table 1
Seismic Lines Used to Construct A-A' and B-B' Sections

Name (–)	References (–)	Orientation (–)	Length (km)	Quality (–)	Cross-section (–)
S6'	Zaafour et al. (2017)	NW-SE	56	Medium	A-A'
Regional TGT-Ghadames	Gabtni et al. (2012)	N-S	~75	Medium	A-A'
Seismic 1	This work	N-S	47.5	High	A-A'
Seismic 2	This work	ENE-WSW	30	High	A-A'
Seismic 3	This work	ENE-WSW	93.5	High	B-B'
Seismic 4	This work	NE-SW	46	High	B-B'
Seismic 5	This work	NE-SW	24.4	High	B-B'
Seismic 5'	This work	NE-SW	40	High	B-B'

Note. These 8 seismic lines have been used for the creation of the sections. The remaining 15 lines were used to get a coherent and harmonized interpretation at the scale of the Jeffara area.

Table 2
Well Database Used to Constrain A-A' and B-B' Section

Code (–)	Date (yr)	TD (m)	TD-ed in (–)	Data type	Perpendicular distance (km)	Cross-section
W1	1955	4,024	Late Permian	Report	1.8	A-A'
W2	1984	2,078	Late Permian	Literature	7.4	A-A'
W3	1987	2,964	Ordovician	Report	17.2	A-A'
W4	1958	2,217	Precambrian	Literature	20.7	A-A'
W5	NoData	3,975	Cambrian	Literature	18.2	A-A'
W5	NoData	3,957	Cambrian	Literature	10.2	B-B'
W6	1962	1,374	Ordovician	Report	11.1	B-B'
W7	1982	819	Cambrian	Report	4.8	B-B'
W8	1958	1,557	Ordovician	Report	8.4	B-B'
W9	1957	1,654	Ordovician	Report	4.2	B-B'
W10	1983	4,247	Cambrian	Report	3.3	B-B'
W11	1966	3,801	Triassic	Literature	6.4	B-B'
W12	NoData	3,160	Jurassic	Literature	10.4	B-B'
W13	1982	1,167	Triassic	Report	26.9	Reference
W14	1956	2,989	Ordovician	Report	21.2	Reference
W15	1959	1,348	Silurian	Report	28.6	Reference

3.1.2. Outcrop Data

We performed structural fieldwork mainly on Permian to Triassic rocks in the Tebaga of Medenine (ToM) and on the Triassic exposures of Jebel Rehach (Figure 2). In the outcrops we focused on bedding positions, on faults and fracture characterization. Faults were analyzed for their attitude and for their movements. Fractures characteristics were collected on well-exposed sub-horizontal surfaces (i.e., pavements of 10s × 10s of meters). The pavements were imaged using a regular camera mounted on a 2.5 m long pole. We photographed the outcrop at regular intervals to obtain good image overlap to assemblage the images using a photogrammetric approach and

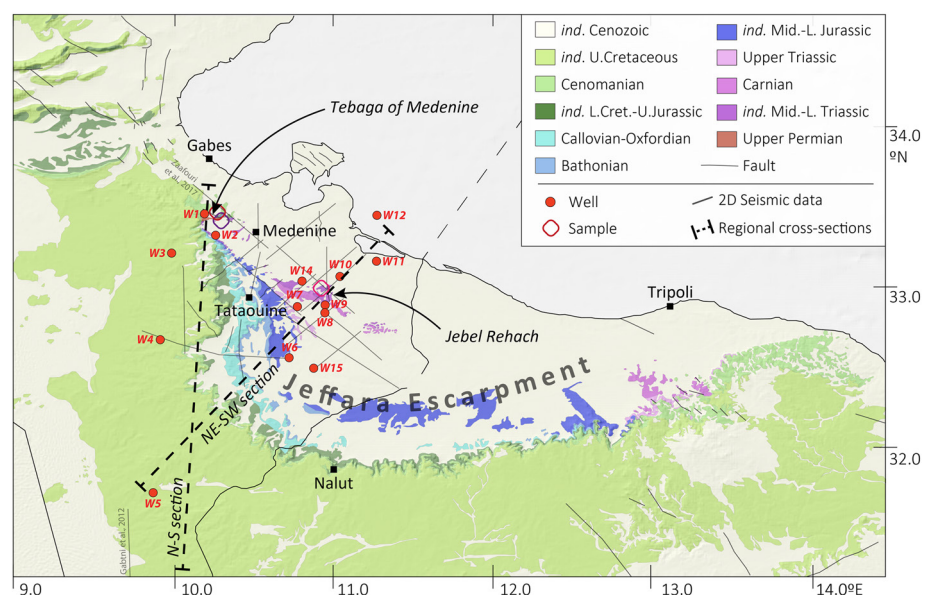


Figure 2. Location of the regional sections (dashed lines) in the area of interest. The map displays the position of the 2D seismic lines and of the wells we used to construct these sections. Geological map is after (Bodin et al., 2010; Raulin et al., 2011).

Table 3

Sample Metadata and Summary of AHe, Apatite Fission Track, ZHe, and Apatite U/Pb Results

Name (–)	Code (–)	Location (–)	Long. (dec.°)	Lat. (dec.°)	Elevation (m)	Stratigraphy (–)	Lithology (–)	Analyses (–)
AFT-P-TM-1	537–01	ToM	10.21717	33.42336	320	Upper Permian	Coarse sdst	U/Pb AFT AHe
AFT-T-TM-2	537–02	ToM	10.259007	33.401417	194	Lower Triassic	Coarse sdst	U/Pb AFT
AFT moonsite	537–03	Rehach	10.930862	32.924109	41	Middle Triassic	Medium sdst	U/Pb ZHe AFT AHe

Note. ToM = Tebaga of Medenine and sdst = sandstone. Mean (U-Th)/He ages are calculated for reproducible aliquots. See Supporting Information S1 for all the produced ages.

obtain digital outcrop models (Corradetti et al., 2017). To our knowledge, this type of acquired geological data is unique in Tunisia. To retrieve the position of layers in the 10s of km large outcrops of the Jeffara escarpment and elsewhere, we acquired systematic bedding measurements in the investigated areas and complemented this ground-based approach with an excel macro from (Martinez-Torres et al., 2012) computing 3-point geological plane extraction from satellite images using TOM African digital elevation model.

3.2. Thermochronology Data

3.2.1. Analytical Methods

We have successfully acquired and extracted new LTT data from outcropping sandstones of the SCJ basin. To our knowledge, this is the first set of publicly available LTT data from the area, part of the reason being that apatite crystals in Permian to Triassic sands are uncommon and have low Uranium content.

The three collected samples (Table 3) yielded datable apatite and zircon crystals. Sample 537-01 was collected in the Upper Permian of the ToM, 537-02 in a Lower Triassic outcrop just south of the ToM, and 537-03 was obtained in a Middle Triassic outcrop of the Jebel Rehach, nearby the Kirchaou locality (Figure 2). Rock samples were crushed (jaw crusher) and minerals separated at Geneva University (Switzerland) using a 300 μ m sieve, a centrifuge (in heavy liquid), and a magnetic separator. Apatite Fission Track (AFT) analyses were carried out at GeoSEP Services with the LA-ICP-MS method. The protocol is summarized in Craddock et al. (2022). AFT ages presented in this work were calculated using the method described in Chew and Donelick (2012). Double dating on crystals was performed for AFT and Apatite U/Pb dating.

We also acquired additional Apatite (U-Th-Sm)/He (AHe) dating for the Permian and Middle Triassic sample (537-01, TM, and 537-03, Jebel Rehach, respectively) and Zircon (U-Th)/He (ZHe) dating for the Permian sample (Table 3). Measurements were performed at the University of Texas at Austin UTChron laboratory following the analytical method of Wolfe and Stockli (2010) and detailed for instance in Colleps et al. (2021). All information can be accessed in Supporting Information S1.

3.2.2. Modeling

Time-Temperature Modeling was performed with the inverse modeling software HeFTy (v2.1.3 of September 2022; (Ketcham, 2005)). HeFTy 2.1 runs Monte Carlo and Controlled Random Search (CRS; (Price, 1977)) algorithms generating user-guided time-temperature paths. Synthetic LTT data are computed for these paths and then compared to measured cooling ages and lengths, resulting in a goodness of fit (GOF; based on the Kolmogorov-Smirnov test). Paths are displayed as “acceptable” when the GOF is between 5% and 50%, and “good” when higher than 50%. The path labeled “best-fit” is the modeling realization that has the highest GOF and thus may change between runs with identical inputs. HeFTy also produces a weighted average curve, which is reproducible between identical runs but does not necessarily yield “acceptable” or “good” values of GOF. In this work, we produced 2 sets of tTMs. One set is using the CRS (presented here in the main text) and the other one the Monte Carlo algorithm (in Supporting Information S1).

HeFTy can run both Monte Carlo and CRS inverse modeling methods while relying on the same LTT raw data. As a sensitivity modeling experiment, we ran both inverse modeling methods to each of our samples with different approach of implementing time/temperature constraints. The methods, boundary conditions, and results are detailed in Supporting Information S1. The results of this experiment were such that, because of their first-order close-similarities between heating and cooling events, we only present the one with the shorter method (i.e., CRS;

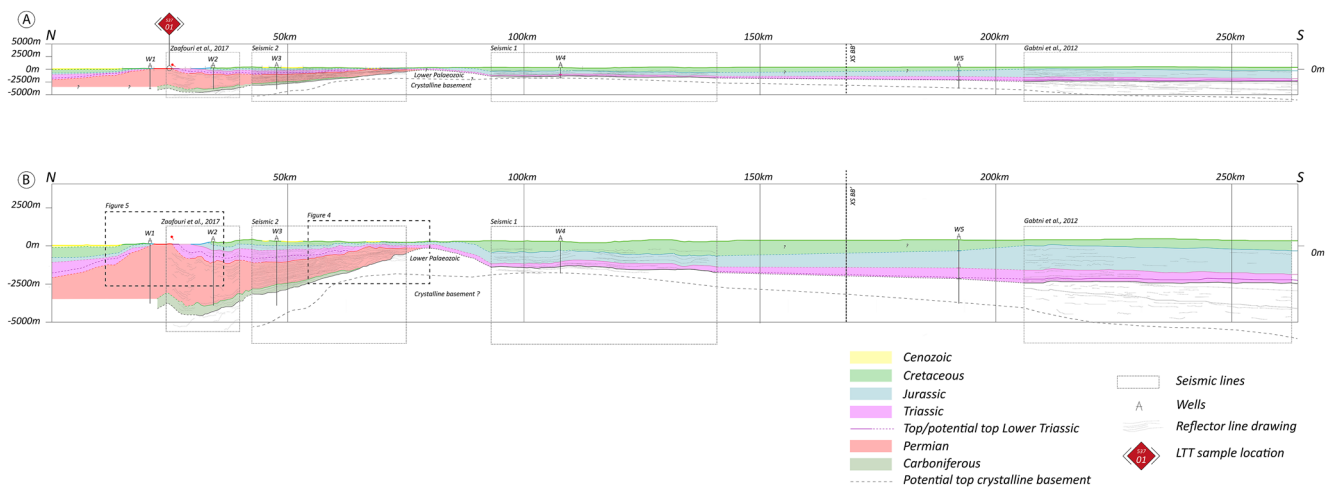


Figure 3. The N-S section. Location shown in Figure 2. (a) without vertical exaggeration, (b) with 1:3 vertical exaggeration. Diamonds indicate the location of collected Low-Temperature Thermochronology sample.

for simplicity's sake and to save manuscript space and reader's time), succinctly in the main text, and describe both methods extensively in Supporting Information S1.

We ran models for the three samples, but it is generally accepted that tracks length data should consist of 50 or more measurements (c.f., “nMTL” in Supporting Information S1; e.g., Donelick & Miller, 1991; Gallagher et al., 1998; Laslett et al., 1984). Samples 537-01 and 537-03 have over 100 measurements and can be reliably used in the tTM (Figure 11). However, sample 537-02 AFT length data set (TM, Lower Triassic) consists of 42 measurements. Therefore, the results of 537-02 should be considered with caution and was thus not added here (see Supporting Information S1).

4. Present Day Architecture of the Southern Chotts-Jeffara Basin

To illustrate effectively the strongly variable 3D geometries of the SCJ basin we present our results based on two regional sections, oriented N-S and SW-NE (Figure 2). The N-S section runs from the area north of the ToM, where it intersects E-W trending folds and faults in the Tebaga (e.g., Mathieu, 1949) to the northern stretches of the Berkine Basin. The SW-NE section runs from the coastal domain near the locality of Zarzis to the vicinity of the town of Remada.

4.1. The N-S Regional Section

4.1.1. General Features

The N-S section stretches for 269 km from the area N of the ToM and ends in the northern regions of the Ghadames Basin in the south. The overall architecture (Figure 3) is well constrained along most of the section, apart from a zone between kilometers 80 and 95 (from north) and a zone between kilometers 140 and 200 further to the south where, however, thicknesses and internal architecture do not display major changes.

4.1.2. Overall Architecture

The most apparent feature of the section is a 10–20 km wide, gentle, asymmetric anticlinal culmination at ca. 80 km from the northern end of the section (Figure 3). As this feature is essentially of pre-Triassic or possibly pre-Carboniferous age, we will name this the Paleozoic culmination. Thickness and architecture of Permian to Jurassic sedimentary successions on the two sides are substantially different. A younger, smaller-scale anticlinal high affecting Permo-Triassic sediments is observed in the north in correspondence with the ToM (see Section 4.1.3). Nowhere along the regional section could we observe major faults disrupting the continuity of formations.

At the northern end of the section, the top of Devonian to Silurian sediments, which forms the base of the sedimentary package addressed in this study, is ca. 4.6 km deep; it then shallows to ca. 1.0 km at the Paleozoic culmination and then deepens very gradually to ca. 2,500 m toward the southern end of the section.

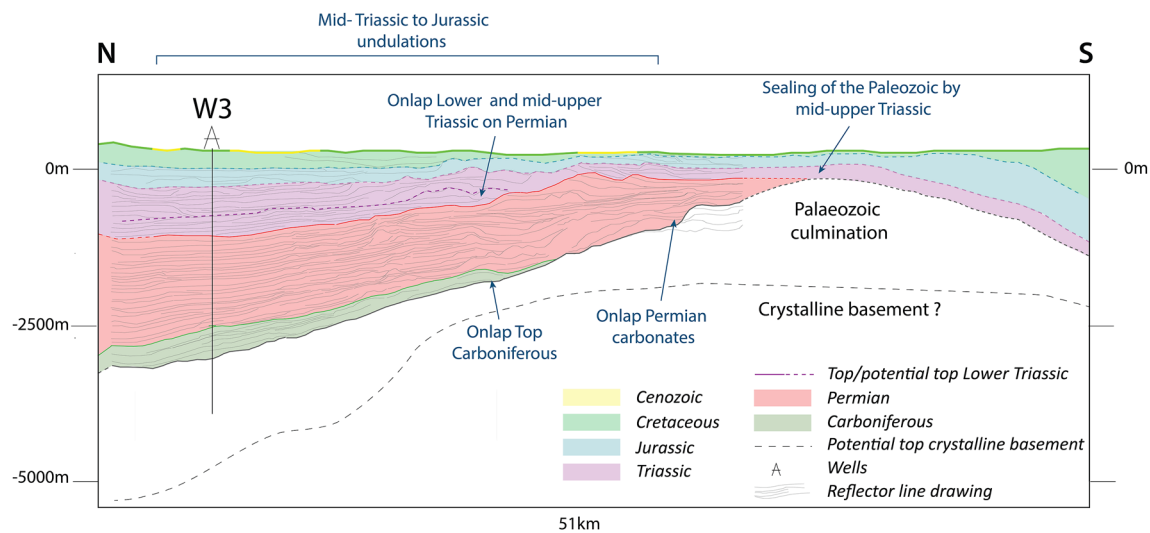


Figure 4. Architecture of northern flank of the Paleozoic culmination. Note the pinch-out and wedges of Carboniferous, Permian, and Triassic sedimentary units.

On the northern side of the culmination, Carboniferous sediments are 0.6 km thick, thin southwards pinching-out ca 20 km north of the culmination and have not been documented in the remaining part of the section (Figure 4).

Permian sediments display major thickness changes: they are >4 km thick in the north (though some of this is possibly a result of tectonic repetition; cf. W1 well initial report), thin toward the south and are only few 100's of meters thick in the vicinity of the culmination, where our seismic data coverage ends. Based on the geometry of internal reflections we assume that they pinch-out at the culmination. No Permian sediments have been documented S of the pinch-out position along the rest of the section (Figure 3). Permian sediments are folded in correspondence of the ToM structure, but their thickness gradually changes and is not impacted by the structure.

Lower Triassic sediments are 0.4 km thick at the northern end of the section and south of the ToM structure from where they gradually thin and seem to onlap the Permian and pinch-out ca 10 km north of the culmination (Figure 4). Lower Triassic sediments have not been stratigraphically documented south of the culmination.

Middle to Upper Triassic sediments show a different architecture and display little changes across most of the section. They are 0.4 km thick in the north, they are deformed and thin slightly across the ToM (see Section 4.1.3), preserve their thickness over the Paleozoic culmination, and further south (W4). Triassic rocks only very gently thicken further to the south and are 0.5 km thick at the southern termination of the line.

Jurassic sediments follow a trend similar to that of Middle to Upper Triassic rocks. Except for the ToM structure, their thickness remains generally constant across the Paleozoic culmination (reaching 0.8 km at well W4) from where it gradually increases toward the south, reaching 1.5 km at the southern termination of the section. Triassic and Jurassic units in the central part of the section (corresponding to the exposures of the Jeffara escarpment) show gentle folding around E-W trending axes.

Lower Cretaceous sediments are generally flat lying, have roughly constant thickness of ca. 0.3 km north of the Paleozoic culmination. South of it they are thicker reaching up to 0.9 km at W4 from where they gradually thin toward the southern termination of the section.

4.1.3. The Tebaga of Medenine (ToM) and Adjacent Regions

The northern part of the regional section traverses the ToM which hosts renowned outcrops which have been object of a long series of studies (e.g., Mathieu, 1949; Raulin et al., 2011; Zaafour et al., 2017). In this work we focus on the structures controlling the development of the ToM inferred from seismic data analysis and from outcrop data.

The ToM (Figures 5 and 6) is a 11 × 6 km large outcrop forming a topographic and geological high generally oriented N080. The central part of the ToM (Figure 6a) is composed of marine Permian deposits (coral bioherms, (Zaafour et al., 2017)). The Permian outcrops are surrounded by Triassic, Jurassic, and Cretaceous sedimentary successions. The western termination of the ToM represents the ideal place to observe the angular relationship

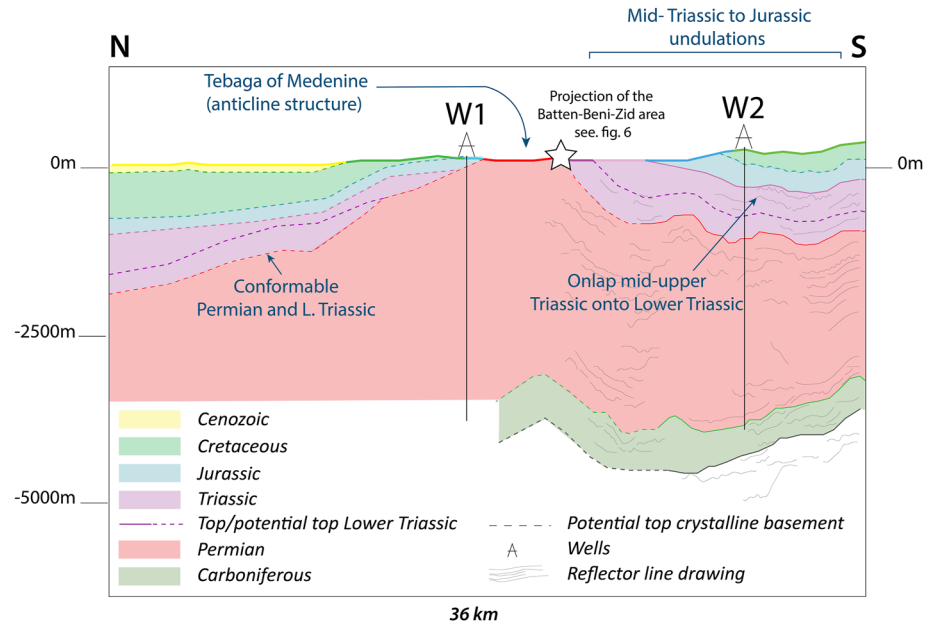


Figure 5. Architecture of the Tebaga of Medenine.

between the different units of the Mesozoic and between the Permian and the Mesozoic succession. In the locality of Ouled M'Halhal, the Cretaceous dipping $1\text{--}2^\circ$ toward the west rests unconformably on the Jurassic units dipping $7\text{--}9^\circ$ southwest (Figure 6b). In the Cheguimi area a spectacular angular unconformity (Bodin et al., 2010; Raulin et al., 2011) is visible between the Permian dipping 23° to 42° S and the Cretaceous dipping $1\text{--}2^\circ$ southwest (Figure 6c). In the Cheguimi sector and directly above the Permian, the base of the Triassic is recognizable and follows the same structural attitude as the Permian (dipping 23° toward the south). In the Chamakh area, an angular unconformity between the base of the Triassic and the Mid-Upper Triassic have been observed. There, the Lower part of the Triassic is still following the same attitude as in the Cheguimi area dipping $21\text{--}23^\circ$ south. This

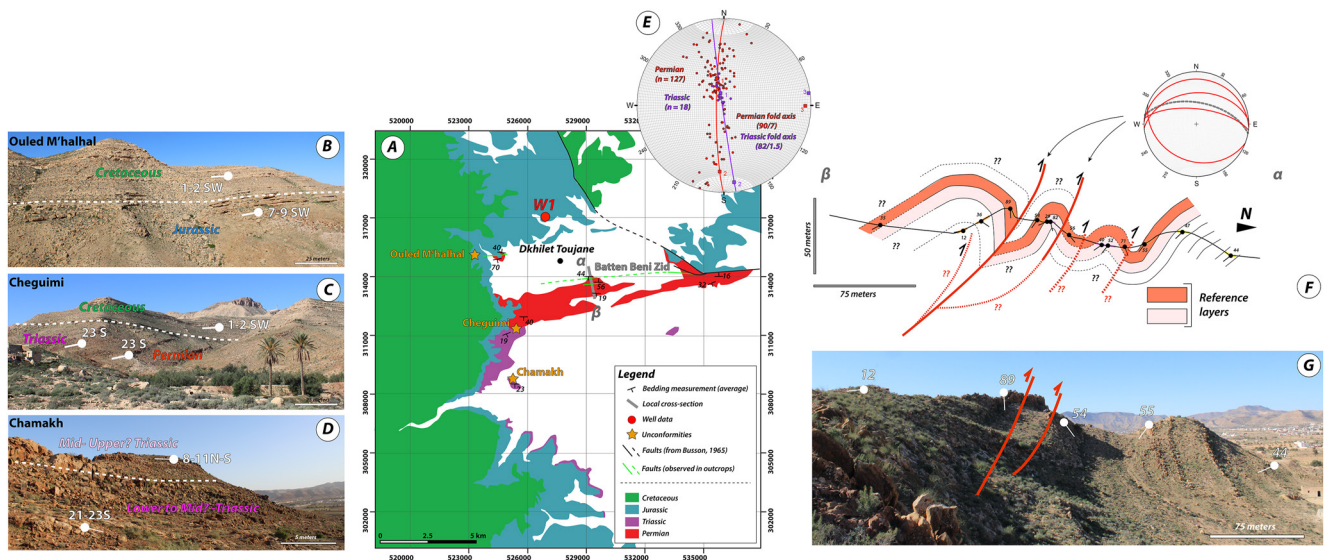


Figure 6. Tebaga of Medenine (ToM) fieldwork synthesis. (a) Location of the ToM and part of the Jeffara escarpment. Localities of mentioned outcrops are indicated; (b) Cretaceous/Jurassic unconformity at the Ouled M'Halhal locality; (c) Cretaceous/Permian and Lower Triassic unconformity at the Cheguimi locality; (d) Intra-Triassic unconformity at the Chamakh locality; and (e) Bedding measurement in the Permian (red) and in the Lower Triassic (purple). (f) Cross-section in the area of Batten-Beni-Zid in the ToM. The stereonet indicates the attitude of faults measured in this location (unfolded according to the present-day bedding attitude); (g) Panorama of the α - β cross-section in the Batten Beni Zid locality.

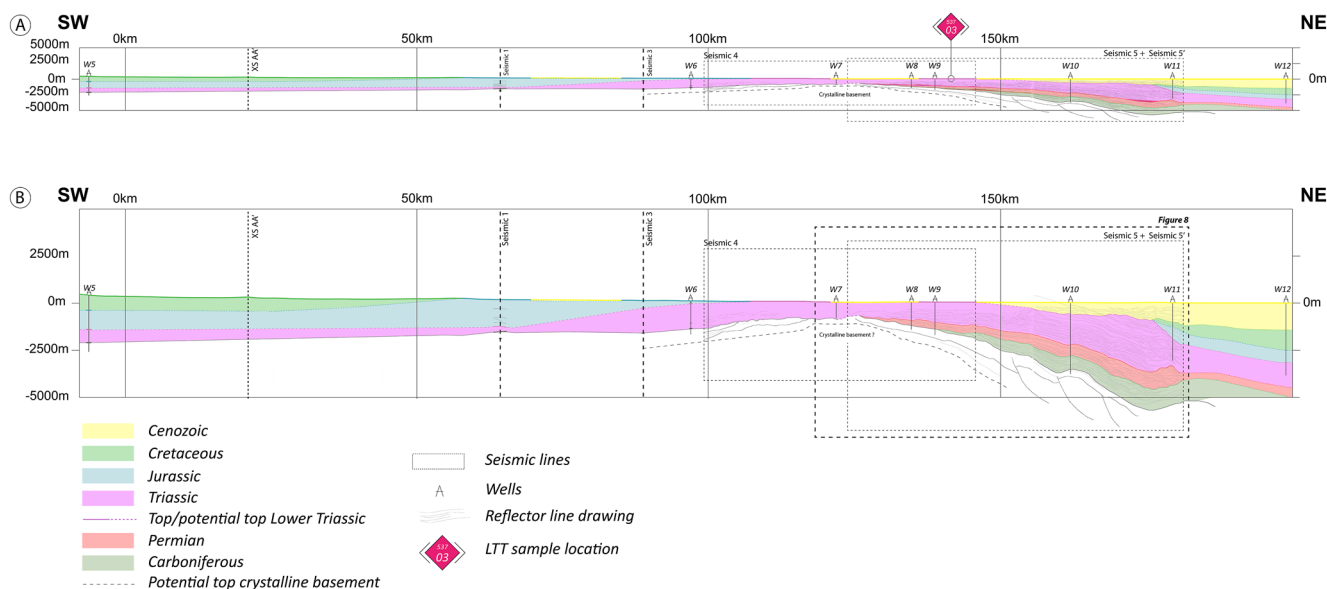


Figure 7. The NE-SW section. Location shown in Figure 2. (a) without vertical exaggeration, (b) with 1:3 vertical exaggeration. Diamonds indicate the location of collected Low-Temperature Thermochronology samples.

Triassic package is overlain by a younger Triassic unit (probably middle-upper Triassic) which has a significantly shallower dip ($8\text{--}11^\circ$) toward the north and the south. This intra-Triassic unconformity has also been observed by Raulin et al. (2011) in the Jebel Rehach where the Carnian rests unconformably on the Lower and Middle Triassic units which in turn are conformable on older underlying rocks. This succession of unconformities attests of complex vertical movements affecting the area of the ToM.

We collected more than 150 bedding measurements on Permian and Lower Triassic units across the ToM. In the northern part of the ToM, Permian beds are dipping toward the north (locally vertical); in the south the same layers dip ca. 30°S . The analysis of the bedding measurements show similar trends and document a fairly symmetric anticline structure with an axis striking N082-N090 (Figure 6e). This overall anticlinal shape is also highlighted by Lower Triassic sediments, which are outcropping on the Chamakh sector, and which have been interpreted from wells and adjacent seismic data in the northern limb. On the northern part of the ToM, the Lower Triassic climbs continuously from >0.75 km depth to the surface, and gently descends toward the south to reach 1.2 km in depth. There is no evidence for any major faults accommodating these changes in depth.

Structural work was conducted in the core of the ToM anticline, in the Batten Beni Zid sector. A 300 m long cross-section (Figures 6f and 6g) displays the existence of a number of 10s of m long, south-verging thrusts causing E-W trending folding (Figure 6b). The reverse faults measured in this area are striking N080-N110 and have a dip varying between 20 and 50° . Similar reverse faults and intense folding have been observed in the Ouled M'Halhal sector (Mathieu, 1949). The ToM is therefore an antiformal stack (Mitra & Boyer, 1986) associated with N-S shortening. Toward the east, the relief of the ToM disappears under flat Cretaceous strata and no apparent trace of the anticlinal stack can be observed at the surface.

The age of the ToM structure is documented by thickness changes and unconformities. While the thicknesses of Permian to Lower Triassic sediments are not affected by the ToM antiformal stack (Figure 6a), this is the case for the Middle Triassic to Jurassic which thin in correspondence of the ToM anticlinal high. The end of deformation is clearly marked by flat lying Lower Cretaceous layers which cover unconformably the ToM structure (Raulin et al., 2011).

4.2. The SW-NE Section

4.2.1. General Features

The NE-SW regional section stretches for 208 km from offshore Zarzis to SW of Remada (Figure 7). Similarly, to the NS section, we find in the NE-SW section the Paleozoic culmination located SW of the Jebel Rehach area. Geometries and stratigraphy NE of the Paleozoic culmination are well-constrained by a number of seismic lines.

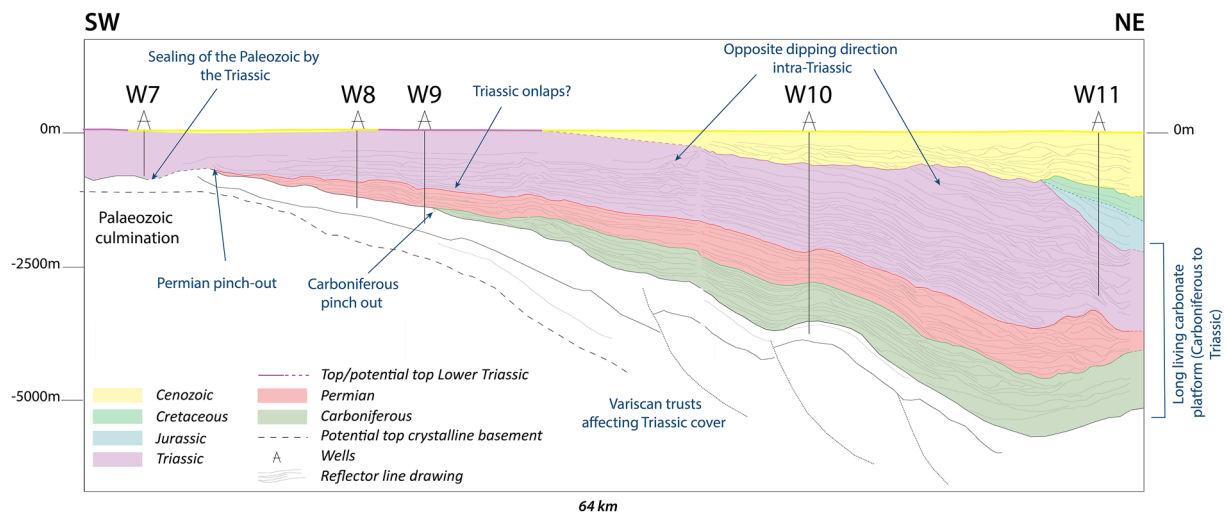


Figure 8. Detail of the NE flank of the Paleozoic culmination along the NE-SW section.

To the SW, on the contrary, the only constraints available are some sparse wells, intersections with 2D seismic lines, and the interpretation carried over at the intersections with the N-S regional section.

The section depicts also a sub-horizontal flank of the Paleozoic culmination to the SW and a steeper, NE limb (up to 11°). There is no evidence for faults accommodating a significant part of the top basement elevation between the crest/core and its flanks.

To the NE, Triassic to Cretaceous sediments form a SW-ward thinning wedge affected by major internal angular unconformities and unconformably capped by gently dipping Tertiary sediments. Carboniferous sedimentary succession at the NE end of the line thins gradually to the SW and pinches-out on the flank of the Paleozoic culmination (Figure 7). A similar pattern is shown by Permian sediments which are ca. 0.9 km thick on the NE flank of the culmination and pinch-out at its top (W9 and W8). Permian and older sediments are affected by a number of SW-verging thrusts which will be described in more detail in Section 4.2.2. No Carboniferous to Permian sedimentary rock has been penetrated by wells to the SW of the Paleozoic culmination.

Triassic sediments (Anisian—Rhaetian (Ghedhoui, 2014)) are at least 2.6 km thick at the northern end of the section (W11) and thin toward the Paleozoic culmination in correspondence of which they are exposed at the surface. Observed thickness, however, is associated with repeated erosional events (preserved in regional unconformity) and does not coincide with the full deposited sedimentary sequence. To the SW of the culmination, a 1.3 km thick Triassic sedimentary unit has been encountered in W6. Based on very sparse data, we infer that Triassic thicknesses slightly decreased toward the SW end of the section. In the most southern well of the section, Triassic sediments are 0.75 km thick (W5).

Jurassic sediments are well documented in the NE but, similarly to Triassic ones, are progressively eroded and disappear slightly to the SW of W5. They are found again SW of the culmination at W6 and seem to thicken substantially in the remaining part of the section.

Cretaceous rocks are lying unconformably on Jurassic and Triassic rocks and being equally unconformably overlain by Tertiary sediments (Figure 8). To the SW of the culmination, Cretaceous rocks appear some 65 km from the culmination and are present until the SW end of the section. In the most southern well of the section, they are ca. 0.8 km thick (W5).

4.2.2. The NE Segment of the Section

The detailed analysis of the NE part of the regional section (Figure 8) provides key elements for the tectonic evolution of the section itself and, at a larger scale, of the SCJ basin. Geometries here are well-constrained by a large number of seismic sections.

Carboniferous and Permian sediments are in conformable contact at the northern end of the section. These units form wedges thinning to the SW and pinching-out ca. 18 km NE of the Paleozoic culmination for the Carboniferous

and at the edge of the culmination itself for the Permian. Internal reflections document the syn-depositional character of tilting.

Triassic sediments lie conformably on top of the Permian and are up to 2.6 km thick in the NE. Their primary thickness, however, cannot be ascertained as the top of the Triassic is everywhere erosional in this part of the basin. Based on the observation that internal reflections are NE dipping but parallel to each other, we assume that the thickness of the Permian (minimum primary thickness) did not change significantly to the SW, toward the Paleozoic culmination.

Jurassic (Hettangian—Sinemurian, (Ghedhoui, 2014; Khouni, 2022)) sediments are present at the NE end of the section (W11), separated by an angular unconformity from the underlying Triassic and capped by another angular unconformity. The mean preserved thickness of Jurassic sediments is 0.6–0.7 km which corresponds to the minimum depositional thickness. The two unconformities join each other a few kilometers from the end of the section marking the disappearance of Jurassic marine rocks. These are then found south of the Paleozoic culmination in outcrops and further SW in the subsurface.

Upper Cretaceous (Cenomanian—Senonian, (Ghedhoui, 2014; Khouni, 2022)) sediments display a similar geometry being bounded at the bottom by the angular unconformity described above and capped by another angular unconformity above which Tertiary (Oligo-Miocene) sediments are found. The two unconformities at the bottom and the top of the Cretaceous merge toward the SW causing the disappearance of Cretaceous rocks ca. 50 km NE of the culmination. Tertiary sediments cover most of the NE part of the section and end ca. 24 km north of the Paleozoic culmination, allowing for the exposure of undifferentiated Triassic continental sedimentary rocks.

Detailed analysis of seismic sections in the area reveals the existence series of SW-verging (on the 2D seismic lines) low-angle thrust surfaces with displacements of 10s to few 100s of meters associated with the development of thrust-related anticlines (Figure 8). These anticlines affect Carboniferous (Dixon et al., 2022) and Permian sediments but also, for instance in the case of the NE-most part of the section, Triassic strata suggesting shortening during this time interval.

4.3. Toward a 3D Scheme

Building on the geologic record presented along the two regional sections, we address here the map-view of our reconstruction presenting estimated primary thickness of Permian to Jurassic sedimentary packages (Figure 9). In the SCJ basin, where sedimentary successions are characterized by major angular unconformities, only part of the originally deposited sediment thickness has been preserved so that presently observed thicknesses may not be representative of original depositional thicknesses and thus should not be used as a proxy for the original geometry of the basin.

4.3.1. Carboniferous to Early Triassic

The two regional sections display a gentle anticlinal high which we named Paleozoic culmination. This culmination delimited a subsiding domain in the N and NE from a stable one in the S until the Early Triassic. Because of their similarities, we assume that the highs imaged along the two sections belong to the same structure which, once plotted on a map, acquires roughly E-W trending direction (Red dashed line, Figure 9).

Carboniferous, Permian and, possibly, Lower Triassic (defined only along the N-S section) sediments are only present in syn-sedimentary wedges to the N and NE of the culmination. In map view (Figure 9), the pinch-out lines positions align along a E-W trend similar to that of the culminations (Ben Ferjani et al., 1990). This confirms the causal relations between the high and the Carboniferous to Lower Triassic wedges.

The position of pinch-outs of Carboniferous, Permian (Figure 9) and Lower Triassic (at least along the N-S section) close the Paleozoic culmination implies that this formed at that time a vertically stable, subdued topographic high separating a subsiding domain in the N from a stable domain in the S where no Carboniferous and Permian sediments were deposited.

4.3.2. Middle (?)/Late Triassic—Jurassic

Differently from the Lower Triassic (where defined) Middle to Upper Triassic sediments are present over the entire region of interest and do not display major thickness changes in correspondence with the Paleozoic culminations. Depositional thicknesses are around 0.5–0.8 km in the west and south and gradually increase toward the NE parts of the study area (2.5 km) (Figure 9).

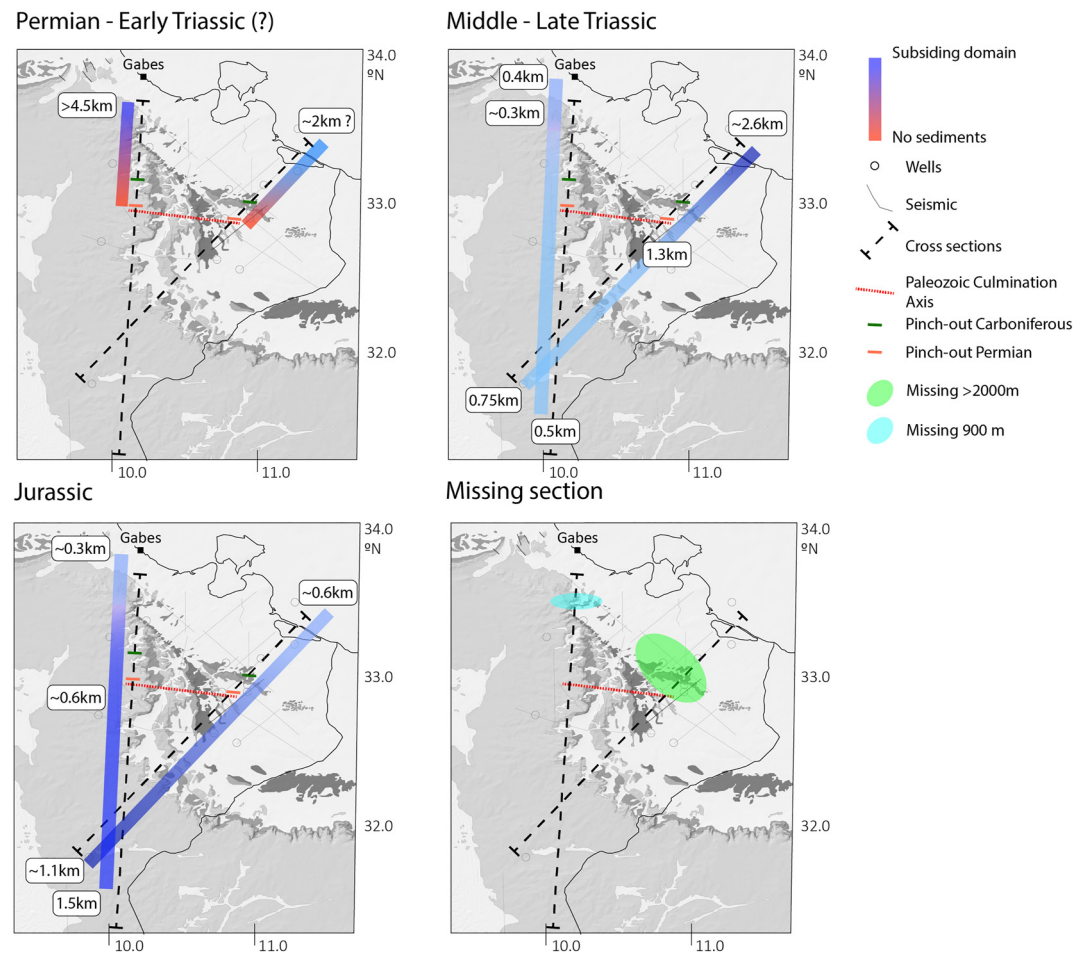


Figure 9. Maps showing semi-quantitative estimates of subsidence in the area of interest based on the two regional sections. Estimates provided in the first three maps refer to (minimum) depositional thicknesses (not including subsequent erosional events). In the map of the missing section, we indicate an estimate of the minimum section missing (see text).

At a more local scale, thicknesses of Middle to Upper Triassic sediments decrease moving toward the ToM contractional high where coeval shortening has been documented by our field work (see Section 3.2.2) as well as previous studies (Bouaziz et al., 2002; Mathieu, 1949; Raulin et al., 2011). Angular unconformities and erosional patterns indicate that the ToM area was gently subsiding only intermittently above sea-level.

Similarly to Middle to Upper Triassic sediments, Jurassic was deposited over most of the area of interest (Figure 9). Primary thicknesses, however, are low in the north and very gradually increase southwards. Further growth of the ToM structure impacted the thickness of Jurassic sediments which thin toward the high.

4.3.3. Stratigraphic Gaps

Using the seismic record (inclusive of the internal reflections) we attempt a semi-quantitative estimate of the amount of erosion which took place before the Early Cretaceous (Figure 9). Erosion in the N-S regional section is recorded in correspondence of the well-known unconformities of ToM (Raulin et al., 2011) and is estimated at least 900 m. Exhumation/erosion had ended in the Early Cretaceous when gentle subsidence affected the region. No exhumation/erosion affected Permian and younger sediments at the Paleozoic culmination. Along the NE-SW regional section, major exhumation and erosion are observed near the Paleozoic culmination, that is, around the region of the Jebel Rehach. Here, we estimate the missing pre-Cretaceous section at more than 2 km probably mostly composed of Triassic rocks (Figure 9). We propose in this paper to call this distinct structural object the Triassic culmination. Based on the supra-crop map of Raulin (2013), we propose that the Triassic culmination extended in NW-SE direction.

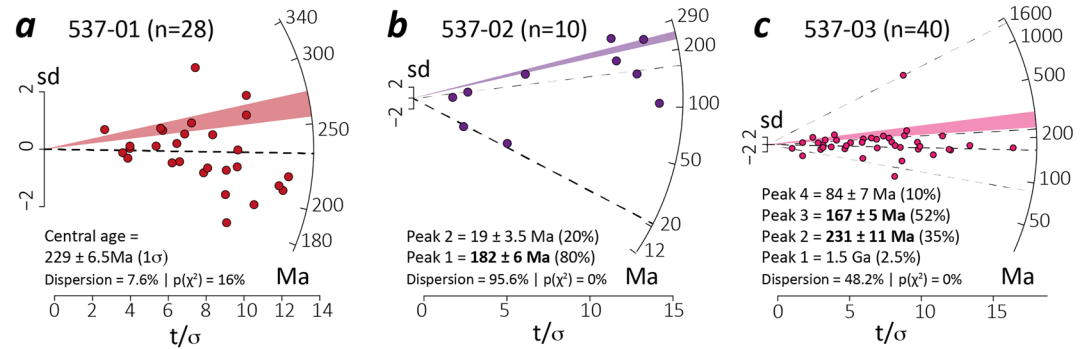


Figure 10. Central Apatite Fission Track age radial plots.

5. Vertical Movements: Inferences From Low Temperature Thermochronology

Estimating geological events taking place during the time interval encompassed by unconformities is a well-known challenge (Green et al., 2022) and this is clearly relevant for the SCJ basin, where large (angular) unconformities are the rule rather than the exception. Low-Temperature Thermochronology (LTT) has proven to be a very powerful tool to unravel downward and upward vertical movements during these stratigraphic gaps.

5.1. LTT Results

Pooled AFT ages fall within the Late Triassic (537-01), the Early Cretaceous (537-02), and the Early Middle Jurassic (537-03) (Table 3, Figure 10, and Supporting Information S1). Samples 537-02 and 537-03 show several single-grain age populations, illustrated as peaks in Figure 10. AFT ages are systematically younger than the stratigraphic units they were measured from showing that the recorded thermal signals refer to post-deposition events and not to those taking place in the sedimentary source areas.

The single grain double dating resulted in new apatite FT (described above) and U-Pb ages (this paragraph, Figure 11). Obtained U-Pb ages are Precambrian to Late Triassic, Precambrian to Cambrian (except for one Late Cretaceous outlier), and Precambrian to Carboniferous (except for one Early Cretaceous outlier), for samples 537-01, 537-02, and 537-03, respectively (Supporting Information S1). For both Triassic samples, obtained ages are significantly older than the stratigraphic ages (except for the two outliers), with mean ages at ca. 515 and 517 Ma (537-02 and 537-03, respectively; failed/poor analyses were removed from the mean calculations; Supporting Information S1). The Permian sample (537-01), on the other hand, is characterized by a much younger mean U-Pb age at ca. 307 Ma, explained by 11 ages equal to - and 7 ages younger than—its stratigraphic age. We interpret this issue as being related to processes like zoning, dissolution/regrowth, and/or recrystallization of the apatite crystals (see Supporting Information S1).

Helium ages of apatites are between 114 and 161 Ma in the TM ($n = 3$) and 48 and 124 Ma in the JR ($n = 8$). Mean ages are 137.5 ± 8.2 Ma for sample 537-01 and 86.2 ± 5.2 Ma for sample 537-03. All AHe ages are younger than the stratigraphy, and statistical ages are significantly younger than for the AFT system.

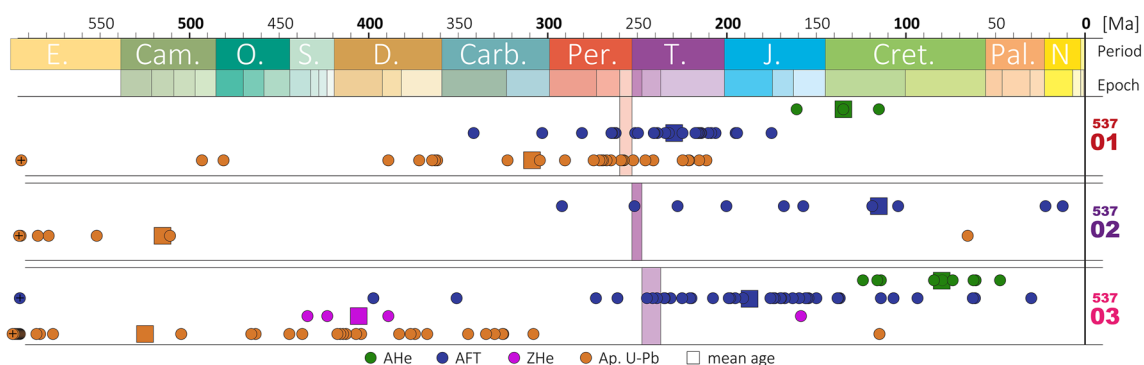


Figure 11. Single grain ages for AHe, Apatite Fission Track, ZHe, and Apatite U-Pb.

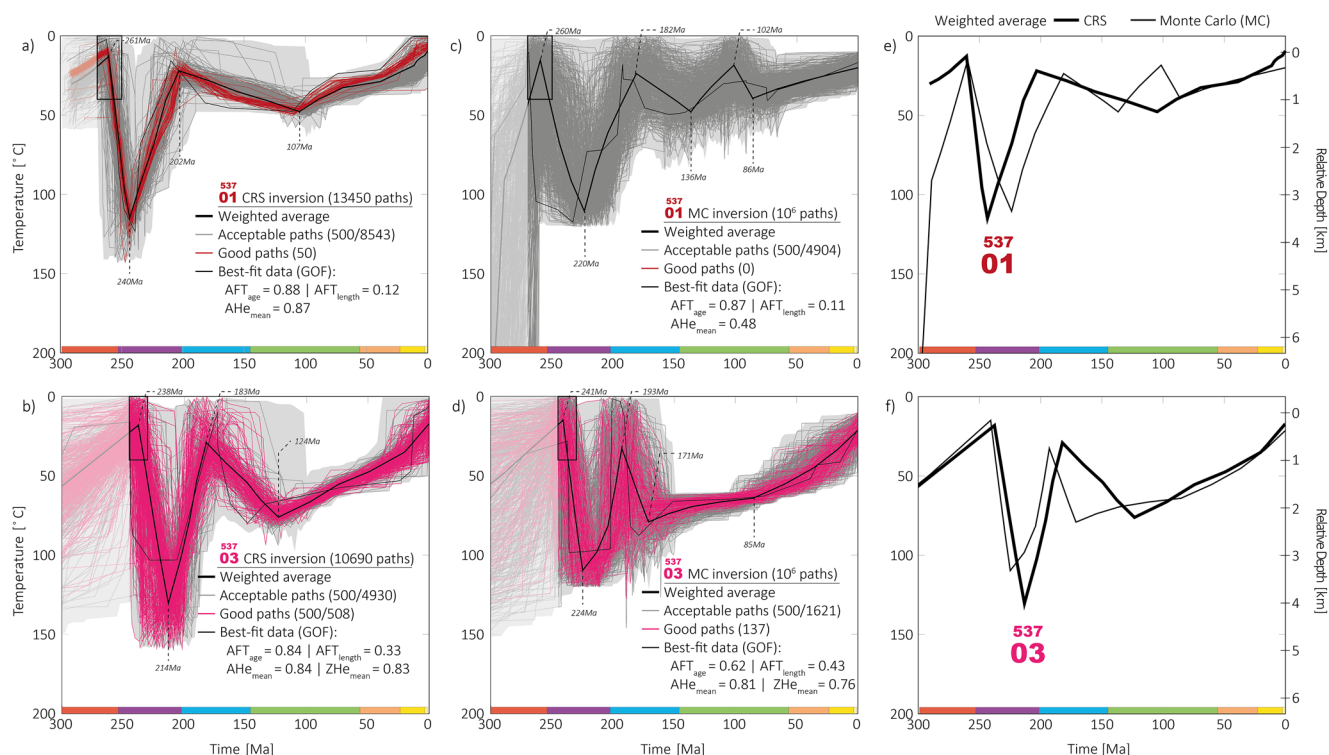


Figure 12. Comparison of the Inverse modeling results obtained HeFTy using the Controlled Random Search (a–c) and the Monte Carlo (d–f) search algorithms. Boxes and modeling parameters are details in the text. Summary and comparison of the weighted average curves (g–i).

Four Zircon (U-Th)/He (ZHe) ages were produced from the Middle Triassic of the Jebel Rehach and are between 160 and 435 Ma. On closer inspection, only one aliquot is younger than the stratigraphic age, at 159.6 ± 12.8 Ma. Median age of 406 Ma likely retains a thermal perturbation from the sedimentary source of the Triassic sediment. The mean age of 352 ± 28.2 Ma has thus no geological meaning, and instead we calculated a mean age for the age cluster older than the stratigraphic age (Figure 11).

5.2. Time-Temperature Modeling Results

Based on the produced forward paths (one per model; manual input of path nodes, which are then tweaked in the x and y directions until “good” GOF value from predicted results are obtained) and adopted modeling constraints, HeFTy runs yielded both acceptable and good paths for all samples (Figure 12). Best-fit results show GOF above 80% for both FT and He dating. Length data show lower values of GOF between 10% and 70%. From the CRS runs, we extracted and display here up to a thousand paths (best-fit, good, and acceptable), weighted average curves, and the acceptable path envelopes.

Sample 537-01 (Permian in the ToM) experienced first heating reaching ca. 120°C, at ca. 240 Ma, then cooling to surface conditions at ca. 200 Ma. A second, less intense, stage of heating followed with the sample reaching ca. 40°C at ~105 Ma (Cretaceous) after which gradually cooled to surface temperatures. Sample 537-03 (Middle Triassic, Jebel Rehach) was first heated reaching ca. 130°C, at ~210 Ma and then cooled to ca. 35°C around 180 Ma. A gentler stage of heating followed which brought sample 537-03 to ca. 65°C, at ~120 Ma (Cretaceous) and then final gradual cooling to the surface.

The two samples follow a remarkably similar path with a strong episode of heating in the Triassic and a much gentler in the Jurassic (Figure 12). At closer inspection, there is a ca. 20 Myr difference in the time when two samples reached the maximum temperatures in the Triassic and when they reached the surface. Jurassic and Cretaceous heating and cooling paths, on the contrary, were similar.

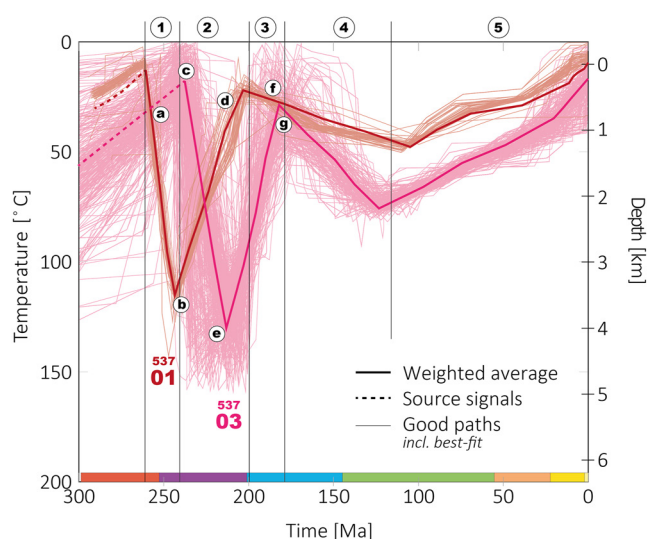


Figure 13. Summary plot of paths for the two samples. Depth conversion has been performed adopting a geothermal gradient of 30°C/km. Circled numbers at the top of the diagram and circled letters along the two curves indicate stages of vertical movements (see text for details).

6. Permian to Early Cretaceous Deformations and Vertical Movements in SCJ Basin

6.1. Integration of Seismic and LTT Data

The integration of seismic and LTT data is essential to derive an interpretation of basin geometries and kinematics during time in areas characterized by downward (subsidence) and upward (exhumation) vertical movements changing in space and time. Seismic data provide valuable information on the magnitude and geometry of subsidence during the deposition of the preserved successions and their relationship with synchronous or subsequent deformation episodes (including tilting). The analysis of internal reflections is of key importance as it allows to discriminate between pre-, syn- and post-tectonic deposition.

LTT provides very essential information on subsidence/exhumation stages. This is valuable when LTT is applied to outcropping samples and combined with seismic interpretation from lines located around the outcrop itself. The overburden of these samples has been eroded and, thereby, direct evidence of vertical movements is missing. The lateral continuation of the overburden missing on top of the sampled outcrops can be interpreted from subsurface data and quantified with LTT. Whether outcropping rocks ever experienced stages of subsidence and exhumation is, a fundamental question which needs to be answered to define the geometry and sedimentology of the basins

during deposition. Areas experiencing exhumation, for instance, were likely to be associated with topographic relief disrupting the previous continuity of the basin and creating drainage partition or areas of sediment erosion and production.

6.2. A Reconstruction

Integrating seismic record (Figures 3 and 7) and LTT (Figure 13) we derive the evolution through time of the two regional sections (Figure 14). Along these sections, the LTT samples are on the syn-tectonic wedge developing north of the Paleozoic culmination (537-01) and close to the high itself (537-03) and are therefore well-suited to provide information on vertical movements and amounts of erosion affecting the region.

In the Late Permian (stage 1a in Figures 13a, 13g, 14a, and 14g) the tectonic wedge is achieved with Carboniferous and Permian sediments pinching-out toward the Paleozoic culmination which acted as a southern boundary for the deposition of the Permian marine sediments. Sample 537-01 had >2 km of Permian sediments underneath it (this is an estimate from the present record reduced to consider the possible tectonic thickening).

At the Middle Triassic, the syn-tectonic wedge became deeper and at ca. 240 Ma (Figure 13 stage 1b and Figure 14b) sample 537-01 reached its maximum depth of ca. 3.5 km burying the bottom of the Permian at depths of >5 km. Overburden was composed of Permian and of subordinate Lower Triassic sediments. Part of this overburden might be associated with thrusting. The Paleozoic culmination was, on the other hand, stable to gently subsiding and it is at this stage that sample 537-03 was deposited (Figure 13 stage 2c Figure 14h). Based on the thrusts observed in the NE-SW section (Figure 14h; Section 4.2.2) we infer a contractional tectonic regime for this time frame.

A major tectonic change affected the area at the Late Triassic time (205 Ma, Figure 13). Shortening affected the northern part of the wedge causing the formation of the ToM structure and bringing sample 537-01 back to the surface (Figure 13 stage 2d and Figure 14c). A substantial exhumation and erosion took place in this stage located a relatively narrow domain of about 10 km width (Figure 5). The lack of seismic data to the north of the ToM does not allow us to infer if the exhuming area extended further to the north.

Away from the ToM, a generalized subsidence phase was affecting the southern part of the area of interest as well as the Jeffara plain toward the east (Figure 13 stage 2e). The Paleozoic culmination experienced generalized subsidence with a magnitude strongly increasing from W (<1 km) to E (>3 km) (section I in Figure 14). Subsidence was affecting therefore a very large area and had a different driving process.

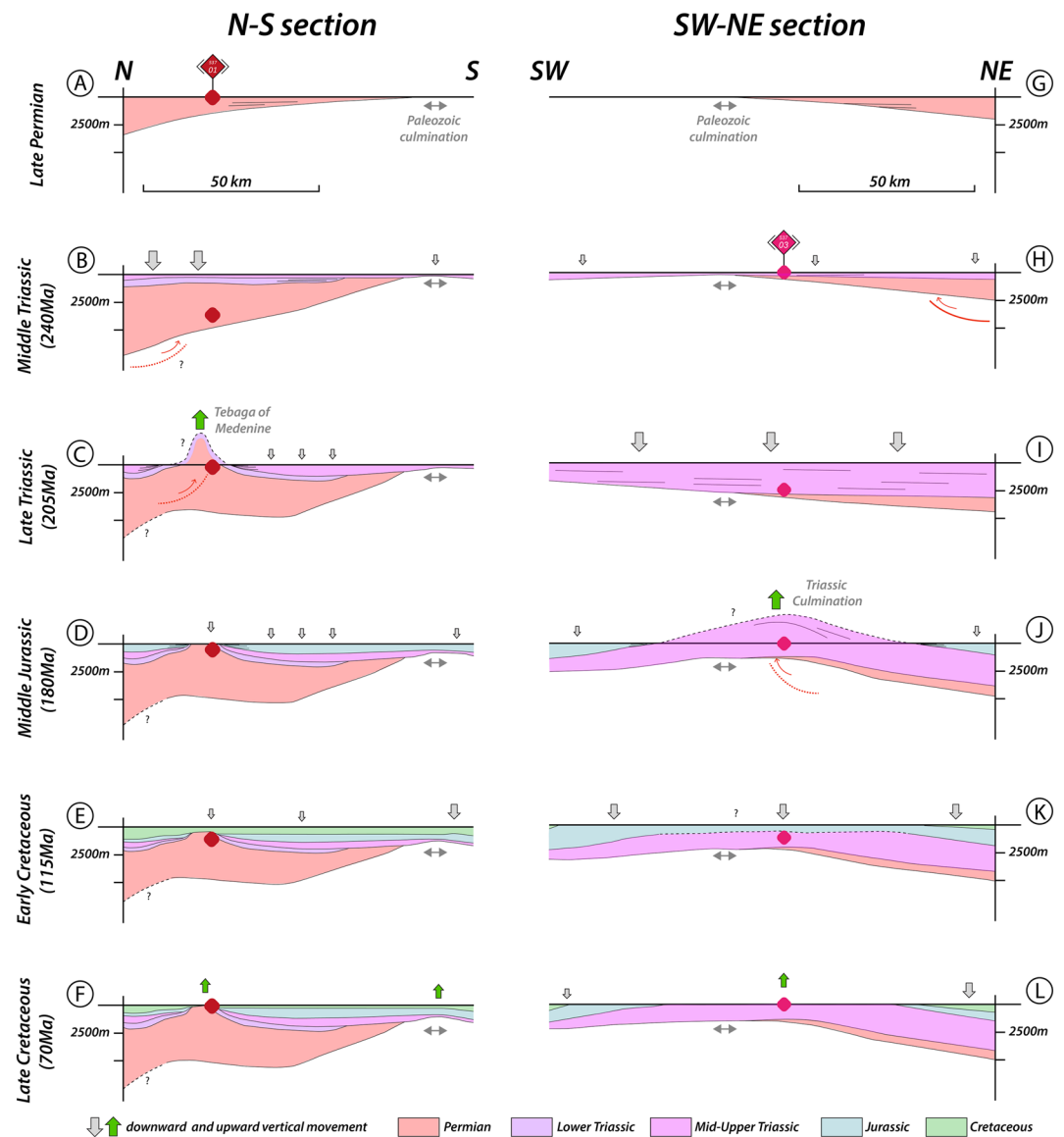


Figure 14. Semi-quantitative geological evolution of the two regional sections constrained by seismic and Low-Temperature Thermochronology (LTT) results. Red and pink diamonds represent the position of the LTT samples through time. Arrows display vertical movements taking place in the time interval before the indicated age. The size of the arrows is proportional to the magnitude of vertical movements.

The Middle Jurassic, 180 Ma (Figure 13 stage 3f) is characterized by substantial changes, quite different along the two sections. Vertical movements along the N-S section (Figure 14d) were limited and a gentle subsidence phase took place. This is in contrast with the NE-SW section (Figure 13 stage 3g and Figure 14j) where the area located north of the Paleozoic culmination experienced major reactivation with the development of a ca. 25 km wide anticline which brought sample 537-03 back to the surface (Figure 13 stage 3g). There is no westward continuation of this structure and, based on previous regional work (Raulin, 2013), we assume that, differently from the ToM, it was oriented NW-SE.

In Early Cretaceous time (115 Ma), generalized subsidence affected the entire area and samples 537-01 and 537-03 reached a depth of ca. 1 and 2 km respectively (Figure 13 stage 4, Figures 14e and 14k). Subsidence increases from west to east.

This subsidence stage is followed by a gentle exhumation phase (Figure 13 stage 5) initiated during the late Cretaceous (70 Ma) and slowly bringing the two collected samples closer to their present-day outcropping position (Figures 14f and 14l).

6.3. A Tectonic Model

6.3.1. The Evolution

During a first stage, from Late Carboniferous to Early Triassic, tectonics led to the formation of a E-W trending, north-ward thickening syn-tectonic wedge N of the Paleozoic culmination. No Carboniferous and Permian sediments were deposited south of this high. At the northern termination of the area of interest, the wedge was 3.5 km thick (Figure 14b) but we do not have enough information to determine its continuation further to the N. There are no major faults controlling the architecture of the wedge. On the other hand, numerous small E-W trending thrust faults are visible in our data and are known from the literature (Figure 9; see isopach map of the Permian at page 34 in Ben Ferjani et al. (1990)). These faults accommodate only displacements which are small with respect to the dimension of the area of interest and these structures document a maximum horizontal stress trending N-S.

At around 230 Ma a new pattern of vertical movements was established leading to (a) the exhumation of the Upper Carboniferous-Permian wedge in the western part of the region inclusive of the development of the ToM structure, and (b) long wavelength regional subsidence in the eastern part of the area of interest. This allowed for the deposition of a >4 km-thick package of Upper Triassic sediments over the entire eastern area irrespective of older structural trends (Figure 14b).

A further change occurred at the Triassic-Jurassic transition. We observe a generalized subsidence in the W in contrast with the exhumation of a several 10s km large area in the east associated with the development of NW-SE trending Triassic culmination (Figure 14j). To the NE of this culmination structure, subsidence was continuing as attested by the development of a syn-tectonic wedge toward the extreme NE of the NE-SW section. We do not have structural information allowing us to precisely confirm the orientation of the axis of the major structure. Further structural work is needed especially in the Jebel Rehach to refine the proposed model.

6.3.2. Basin Formation Mechanisms

According to our observations, vertical movements (subsidence and exhumation) are controlled by regional, large wavelength processes and that faults play a subordinate role. Even features such as the ToM and Triassic culmination are essentially anticlines which developed in a shortening regime. Most faults we have observed are small and contractional in nature and document a compressional stress regime during basin formation. Defining and quantifying relevant tectonic processes is, however, challenging because of the repeated stages of km-scale exhumation which disrupted the primary sedimentary successions making it impossible to use present day thickness data to infer basin geometries.

The first tectonic stage is relatively simple and characterized by the formation of a syn-tectonic wedge opening toward the north. Such a wedge could be the southernmost segment of a Late Variscan foredeep. This interpretation is supported by Dixon et al. (2010) and Simancas et al. (2005) but is potentially at odds with the observation that the main phase of Variscan thrusting and mountain building in north Africa took place in the Late Carboniferous. If, however, the Variscan collision between Laurussia & Gondwana was diachronous, “younging” toward the east then a Permian Foredeep in southern Tunisia might be a possibility.

During the first part of the second stage, exhumation of the sedimentary wedge in the west was coeval with generalized subsidence in the E. This was followed by a stage when the western domains were stable while major exhumation took place in the E with the development of the NW-SE trending Jebel Rehach anticline. Eventually the entire region experienced <1.5 km of subsidence until the late Early Cretaceous followed by generalized exhumation.

7. Discussion

7.1. Impact on Sedimentary Systems

In the tectonic model we propose, two large scale structures developed which experienced substantial exhumation, one in the ToM (Middle Triassic) and one associated with the Triassic culmination (Late Triassic). Kilometer-scale exhumation as documented here is necessarily associated with the development of a topographically elevated

region which disrupted the continuity of the coeval sedimentary basins and provided a local source for Triassic sediments. Fortunately, Triassic sediments of southern Tunisia have been well studied at local and regional (incl., depositional context in Algeria and Libya; (El Fandi, 2012; Moustafa et al., 2019)) and information concerning their lithology, sedimentology (including palaeocurrents), stratigraphy and palaeontology is readily available (e.g., Ben Ferjani et al., 1990; Kamoun et al., 2001; Soussi et al., 2017). The ToM and the Triassic culmination divide the Triassic into two distinct depositional regions into the SCJ basin: (a) a western region dominated by a significant volcanic province (extending west into Algeria) where volcanics and volcanoclastic strata are interbedded with fluvial sandstones, and (b) an eastern region without volcanics and dominated by fluvial sandstones (extending east into Libya). Subsurface data (2D seismic profiles and wells) confirm that the culminations are on-lapped by the Lower Triassic sediments on both their western and eastern margins. In the Triassic outcrops in the vicinity of ToM, palaeocurrent data in Bibonne (2014) show flow toward the ESE corroborating our findings that the ToM was a positive feature at this time (Figure 14c). In the Triassic outcrop belt of the Jebel Rehach, paleocurrents along the outcrop are generally toward the north and north-east, (Bibonne, 2014) and sedimentological analysis suggests a major, multi-story, fluvial channel system is probably influenced by the Triassic culmination (Figure 14j).

7.2. Distributed (Inelastic) Deformation in Permian and Triassic Rocks

Forelands of compressional orogens and lithospheric plates experiencing buckling (Raimondo et al., 2014) are typically characterized by high levels of far field stresses propagating over very large distances. Such high stresses might cause widespread inelastic deformation even in the absence of large-scale tectonic structures. Inelastic deformation is typically accommodated by regional networks of fractures with little displacements which have a profound effect on physical properties of rocks such as permeability. Fracture networks have been rarely described from Tunisia (Bouaziz et al., 2002), but they are quite common. They are, for instance, very apparent in the region of the ToM and of the Jebel Rehach (localization on Figure 2).

To test the hypothesis of inelastic deformation, we have conducted preliminary investigations in outcrops located in the ToM and the Jebel Rehach. Our work shows that distributed fractures are organized in networks consisting of pairs of conjugate fractures and of stylolites (Figure 15). The geometry of the network points to a ca. N-S oriented σ_1 and E-W oriented σ_3 , compatible with the stresses which caused Middle-Late Triassic shortening in the ToM.

In the ToM region we observed conjugated sets of fractures, associated with tectonic stylolites oriented E-W (Figure 15 A-A'). As the pavements with the associated fractures have been steepened during Middle Triassic shortening, we conclude that fractures also developed in the same time frame. The fractures observed in the Middle Triassic of the Jebel Rehach area (Figure 15 B-B') show a similar type of organization. If the shortening interpretation is confirmed, it would suggest that this Triassic event caused widespread development of consistent fracture networks in large portions of central Tunisia.

8. Conclusion

In this study we have presented the results of our analysis of outcrops and of a large set of seismic sections. One of the most apparent features of our data is the widespread occurrence of angular unconformities. Those unconformities document the important erosional events which have affected at various times large parts of the primary successions deposited in the SCJ basin. The erosion we describe here, implies that presently observed thicknesses can be substantially different (less) than the primary ones. We have, therefore, integrated subsurface data interpretation with LTT to document time relations between deposition and deformation and to quantify the magnitude of thermal events which were translated into burial and exhumation.

We have presented the results of our work along two regional sections, oriented N-S and NE-SW. The two sections illustrate a syn-sedimentary wedge in the north composed of Carboniferous to Lower Triassic sediments pinching out against an EW trending Paleozoic culmination. During the beginning of the Lower Triassic, around the present-day ToM, the upper Permian was buried at more than 5 km. This burial episode has potentially strong implications for hydrocarbon systems in terms of maturity. At around 230 Ma, the ToM developed associated with the onset of a N-S oriented phase of shortening. At the same time, the eastern domain was subsiding allowing for the deposition of more than 4 km of Triassic sediments toward the NE, in the Jeffara plain. At around 180–170 Ma, an exhumation phase affected the NE part of the area of interest giving raise to the local Triassic culmination. The ToM and the Triassic culmination are temporally and spatially disconnected structures.

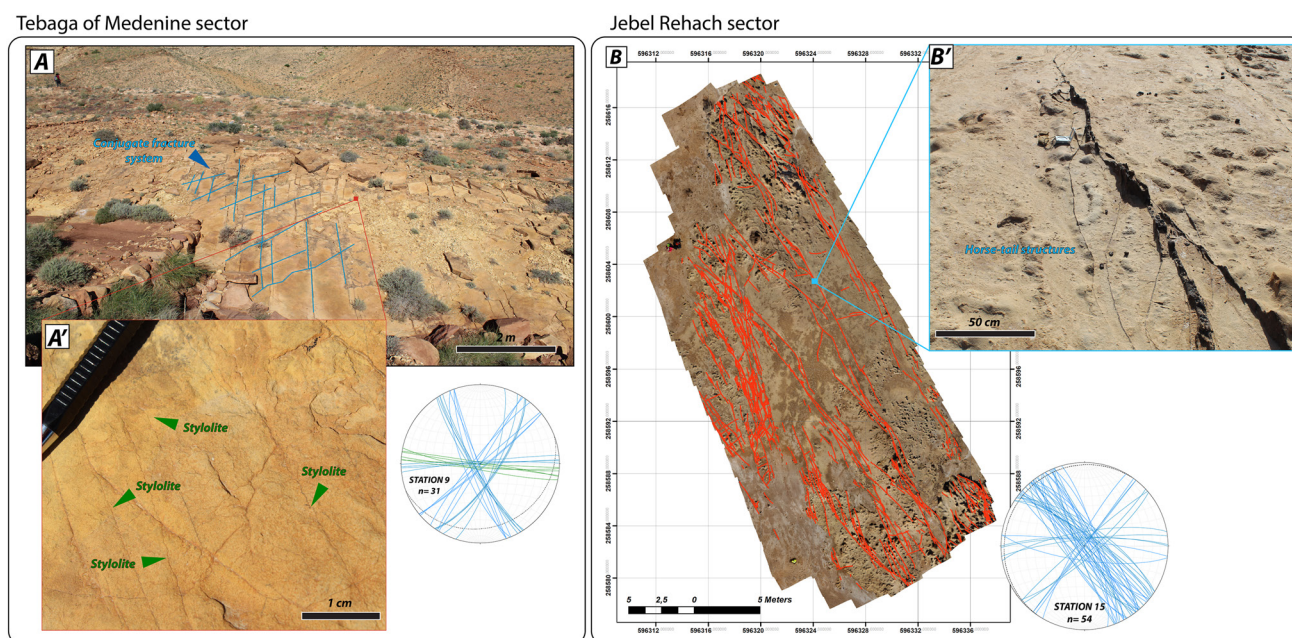


Figure 15. (a) Fractures on a Permian pavement in the Tebaga de Medenine forming. Conjugate pairs associated with tectonic stylolites (A'). (b) Lower Triassic pavement (e.g., bedding parallel 2D outcrop surface) with interpreted fractures in the Jebel Rehach area. B') Fracture with horse tail structure.

Our observations show that vertical movements in Southern Tunisia are essentially controlled by large wavelength and low amplitude anticlines structures emplaced under shortening regime. In this configuration, we observe that faults play only a subordinate role on the structuring of the SCJ basin.

Data Availability Statement

The raw Low Temperature Thermochronology (LTT) data, the fieldwork data set collected in the Tebaga of Medenine and in the Jebel Rehach (incl. measurements, images of large horizontal outcrops (such as the one displayed in Figure 15) and location of measurement station in GIS format) are archived into our institute trusted and certified 4TU.ResearchData repository under the reference “Low temperature thermochronology and outcrop geology data from the Jeffara region, Southern Tunisia” (Bruna et al., 2023). The software used for the modeling of LTT data (HeFTy) is a FAIR-compatible open-source software (v2.1.3 of September 2022, (Ketcham, 2005)). The regional section presented in this paper were constrained by several seismic lines and well data. Two of the used seismic lines (in the NS section) come from literature (Gabtni et al., 2012; Zaafouri et al., 2017). The rest of the seismic lines (6 lines) and the totality of the well data (15 boreholes) are confidential data provided by the supporting company (Mazarine Energy B.V.). Those data have been provided in the form of seg-y for the seismic lines and scanned confidential reports or extract of internal documents (referred in table 2 as literature, property of Mazarine Energy B.V.) for the borehole data.

References

- Acheche, M. H., M'Rabet, A., Ghariani, H., Ouahchi, A., & Montgomery, S. L. (2001). Ghadames basin, southern Tunisia: A reappraisal of triassic reservoirs and future prospectivity. *AAPG Bulletin*, 85(5), 17.
- Ben Ferjani, A., Burollet, P. F., & Mejri, F. (1990). *Petroleum geology of Tunisia*. Entreprise Tunisienne d'Activites Petrolieres.
- Bertotti, G., & Gouiza, M. (2012). Post-rift vertical movements and horizontal deformations in the eastern margin of the Central Atlantic: Middle Jurassic to Early Cretaceous evolution of Morocco. *International Journal of Earth Sciences*, 101(8), 2151–2165. <https://doi.org/10.1007/s00531-012-0773-4>
- Bibonne, R. (2014). *Sédimentologie et stratigraphie des séries clastiques du Trias inférieur à moyen du bassin de Ghadamès et de la Jeffara (Tunisie et Libye)* 250. University of Strasbourg.
- Bodin, S., Petitpierre, L., Wood, J., Elkanouni, I., & Redfern, J. (2010). Timing of early to mid-cretaceous tectonic phases along North Africa: New insights from the Jeffara escarpment (Libya-Tunisia). *Journal of African Earth Sciences*, 58(3), 18–506. <https://doi.org/10.1016/j.jafrearsci.2010.04.010>
- Bouaziz, S., Barrier, E., Soussi, M., Turki, M. M., & Zouari, H. (2002). Tectonic evolution of the northern African margin in Tunisia from paleostress data and sedimentary record. *Tectonophysics*, 357(1), 227–253. [https://doi.org/10.1016/s0040-1951\(02\)00370-0](https://doi.org/10.1016/s0040-1951(02)00370-0)

Acknowledgments

We thank the sponsors of the North Africa Research Group (NARG) for the funding of this research. Mazarine Energy B.V. is thanked for providing access to well and seismic data. Geologists from Mazarine Energy Tunisia, ETAP, ONM, and from the University of Tunis El Manar are greatly thanked for their time in the field and constructive discussions. We would like to thank Andrea Moscaricello and Diego Villagomez from The University of Geneva for the preparation of the LTT samples, Paul O'Sullivan from GeoSEP for the AFT analyses and Daniel Stockli from the University of Texas at Austin for the ZHe analyses. We would like to thank Ruaridh Smith from the University of Erlangen-Nurnberg and Christos Kougioulis for their MSc research works on the Jeffara area. We would like to thank François Roure and an anonymous reviewer as well as the editor of Tectonics, Laurent Jolivet for their comments which improved the quality of the paper.

- Bruna, P.-O., Charton, R., & Bertotti, G. (2023). Low temperature thermochronology and outcrop geology data from the Jeffara region, Southern Tunisia. Version 1 [Dataset]. 4TU.ResearchData. <https://doi.org/10.4121/aa453712-b36f-4f01-98b8-e9f0517d2052>
- Burrollet, P. F. (1991). Structures and tectonics of Tunisia. *Tectonophysics*, 195(2), 359–369. [https://doi.org/10.1016/0040-1951\(91\)90221-d](https://doi.org/10.1016/0040-1951(91)90221-d)
- Chamot-Rooke, N., Ragin, C., & Le Pichon, X. (2005). *A synthesis of deep marine data in eastern Mediterranean* (Vol. 64). Mémoires de la Société géologique de France.
- Chew, D. M., & Donelick, R. A. (2012). Combined apatite fission track and U-Pb dating by LA-ICP-MS and its application in apatite provenance analysis. In *Quantitative mineralogy and microanalysis of sediments and sedimentary rocks: Mineralogical association of Canada*. Short Course.
- Colleps, C. L., McKenzie, N. R., Guenther, W. R., Sharma, M., Gibson, T. M., & Stockli, D. F. (2021). Apatite (U-Th)/He thermochronometric constraints on the northern extent of the Deccan large igneous province. *Earth and Planetary Science Letters*, 571, 117087. <https://doi.org/10.1016/j.epsl.2021.117087>
- Corradetti, A., Tavani, S., Russo, m., Arbues, P. C., & Granado, P. (2017). Quantitative analysis of folds by means of orthorectified photogrammetric 3D models: A case study from Mt. Catria, northern Apennines, Italy. *Photogrammetric Record*, 17.
- Craddock, W. H., O'Sullivan, P. B., & McAleer, R. J. (2022). U-Pb and fission-track data from zircon and apatite resolve latest- and post-Alleghanian thermal histories along the Fall Line of the Atlantic margin of the southeastern United States. *Geosphere*, 18(4), 1330–1353. <https://doi.org/10.1130/GES02447.1>
- Dixon, R. J., Kougioulis, C., Bruna, P.-O., Charton, R., Hollis, C., Bulot, L., et al. (2022). Carboniferous marine carbonate sequences of southern Tunisia: Seismic stratigraphy, depositional facies & petroleum systems: Implications for the North African margin. In *Africa conference, the future of G&G in Africa's E&P: Skills, transition & Resources*. HGS-PESGB.
- Dixon, R. J., Moore, J. K. S., Bourne, M., Dunn, E., Haig, D. B., Hossack, J., et al. (2010). Integrated petroleum systems and play fairway analysis in a complex Palaeozoic basin: Ghadames-Illizi Basin, North Africa. In B. A. Vining & S. C. Pickering (Eds.), *Petroleum geology: From mature basins to new Frontiers – proceedings of the 7th petroleum geology conference*. Geological Society of London.
- Donelick, R. A., & Miller, D. S. (1991). Enhanced TINT fission track densities in low spontaneous track density apatites using 252Cf-derived fission fragment tracks: A model and experimental observations. *International Journal of Radiation Applications and Instrumentation - Part D: Nuclear Tracks and Radiation Measurements*, 18(3), 301–307. [https://doi.org/10.1016/1359-0189\(91\)90022-A](https://doi.org/10.1016/1359-0189(91)90022-A)
- El Fandi, E. (2012). *Early Mesozoic stratigraphy, sedimentology and structure of the Gharian area* (p. 397). Plymouth University.
- Eschard, R., Braik, F., Bekkouche, D., Rahuma, M. B., Desaubliaux, G., Deschamps, R., & Proust, J. N. (2010). Palaeohighs: Their influence on the North African palaeozoic petroleum systems. In *Petroleum geology: From mature basins to new Frontiers – proceedings of the 7th petroleum geology conference*. Geological Society of London.
- Frizon de Lamotte, D., Raulin, C., Mouchot, N., Wrobel-Daveau, J.-C., Blanpied, C., & Ringenbach, J.-C. (2011). The southernmost margin of the Tethys realm during the Mesozoic and Cenozoic: Initial geometry and timing of the inversion processes. *Tectonics*, 30(3), TC3002. <https://doi.org/10.1029/2010tc002691>
- Gabtni, H., Alyahyaoui, S., Jallouli, C., Hasni, W., & Mickus, K. L. (2012). Gravity and seismic reflection imaging of a deep aquifer in an arid region: Case history from the Jeffara basin, southeastern Tunisia [Dataset]. *Journal of African Earth Sciences*, 66–67, 85–97. <https://doi.org/10.1016/j.jafrearsci.2012.03.007>
- Gabtni, H., Jallouli, C., Mickus, K. L., Zouari, H., & Turki, M. M. (2009). Deep structure and crustal configuration of the Jeffara basin (Southern Tunisia) based on regional gravity, seismic reflection and borehole data: How to explain a gravity maximum within a large sedimentary basin? *Journal of Geodynamics*, 47(2), 142–152. <https://doi.org/10.1016/j.jog.2008.07.004>
- Gallagher, K., Brown, R., & Johnson, C. (1998). Fission track analysis and its applications to geological problems. *Annual Review of Earth and Planetary Sciences*, 26(1), 519–572. <https://doi.org/10.1146/annurev.earth.26.1.519>
- Gharbi, M., Masrouhi, A., Espurt, N., Bellier, O., Amari, E. A., Ben Youssef, M., & Ghanmi, M. (2013). New tectono-sedimentary evidences for Aptian to Santonian extension of the Cretaceous rifting in the northern Chotts range (southern Tunisia). *Journal of African Earth Sciences*, 79, 16–73. <https://doi.org/10.1016/j.jafrearsci.2012.09.017>
- Ghedhoui, R. (2014). *Apports de l'imagerie sismique et des SIG à l'étude morphostructurale de la Jeffara (Sud Est tunisien): Implications géodynamiques et intérêts pétroliers* (p. 265). Université Paris-Est Marne-La-Vallée.
- Ghorbal, B., Bertotti, G., Foeken, J., & Andriessen, P. (2008). Unexpected Jurassic to Neogene vertical movements in “stable” parts of NW Africa revealed by low temperature geochronology. *Terra Nova*, 20(5), 9–363. <https://doi.org/10.1111/j.1365-3121.2008.00828.x>
- Gouiza, M., Bertotti, G., Charton, R., Haimoudane, K., Dunkl, I., & Anczkiewicz, A. (2019). New evidence of “anomalous” vertical movements along the hinterland of the Atlantic NW African margin. *Journal of Geophysical Research: Solid Earth*, 21. <https://doi.org/10.1029/2019JB017914>
- Green, P., Duddy, I., & Japsen, P. (2022). Episodic kilometre-scale burial and exhumation and the importance of missing section. *Earth-Science Reviews*, 234, 104226. <https://doi.org/10.1016/j.earscirev.2022.104226>
- Guiraud, R., Bosworth, W., Thierry, J., & Delplanque, A. (2005). Phanerozoic geological evolution of northern and central Africa: An overview. *Journal of African Earth Sciences*, 43(1), 83–143. <https://doi.org/10.1016/j.jafrearsci.2005.07.017>
- Kamoun, F., Peybernès, B., Ciszak, R., & Calzada, S. (2001). Triassic palaeogeography of Tunisia. *Palaeogeography, Palaeoclimatology, Palaeoecology*, 172(3), 223–242. [https://doi.org/10.1016/s0031-0182\(01\)00283-8](https://doi.org/10.1016/s0031-0182(01)00283-8)
- Ketcham, R. A. (2005). Forward and inverse modeling of low-temperature thermochronometry data [Software]. *Reviews in Mineralogy and Geochemistry*, 58(1), 275–314. <https://doi.org/10.2138/rmg.2005.58.11>
- Khouini, R. (2022). *Etude structurale et reconstitution de l'histoire géodynamique de la Jeffara-Tunisie méridionale au cours du Mésozoïque et du Cénozoïque* (p. 276). Université de Tunis El Manar.
- Laslett, G. M., Gleadow, A. J. W., & Duddy, I. R. (1984). The relationship between fission track length and track density in apatite. *Nuclear Tracks and Radiation Measurements*, 9(1), 29–38. [https://doi.org/10.1016/0735-245X\(84\)90019-X](https://doi.org/10.1016/0735-245X(84)90019-X)
- Lubeseder, S., Redfern, J., Petitpierre, L., & Fröhlich, S. (2010). Stratigraphic trapping potential in the carboniferous of North Africa: Developing new play concepts based on integrated outcrop sedimentology and regional sequence stratigraphy (Morocco, Algeria, Libya). In B. A. Vining & S. C. Pickering (Eds.), *Petroleum geology: From mature basins to new Frontiers – proceedings of the 7th petroleum geology conference*. Geological Society of London.
- Martinez-Torres, L. M., Lopetegui, A., & Eguiluz, L. (2012). Automatic resolution of the three-points geological problem. *Computers & Geosciences*, 42, 200–202. <https://doi.org/10.1016/j.cageo.2011.08.031>
- Mathieu, G. (1949). *Contribution à l'étude des Monts Troglodytes dans l'Extrême Sud Tunisien* (p. 82). Régence de Tunis.
- Mitra, G., & Boyer, S. E. (1986). Energy balance and deformation mechanisms of duplexes. *Journal of Structural Geology*, 8(3), 291–304. [https://doi.org/10.1016/0191-8141\(86\)90050-7](https://doi.org/10.1016/0191-8141(86)90050-7)

- Moustafa, M. S. H., Pope, M. C., & Mriheel, I. Y. (2019). High resolution sequence stratigraphy of the Middle–Late Triassic Al Aziziyah formation, northwest Libya. *Journal of African Earth Sciences*, 155, 75–89. <https://doi.org/10.1016/j.jafrearsci.2019.03.009>
- Price, W. L. (1977). A controlled random search procedure for global optimisation. *The Computer Journal*, 20(4), 367–370. <https://doi.org/10.1093/comjnl/20.4.367>
- Raimondo, T., Hand, M., & Collins, W. J. (2014). Compressional intracontinental orogens: Ancient and modern perspectives. *Earth-Science Reviews*, 130, 128–153. <https://doi.org/10.1016/j.earscirev.2013.11.009>
- Raulin, C. (2013). *De l'Afrique du Nord au bassin Sud Tunisien: Histoire tectonique du bassin Sud-tunisien (Jeffara) du Paléozoïque au Tertiaire*. Université de Cergy-Pontoise.
- Raulin, C., Frizon de Lamotte, D., Bouaziz, S., Khamsi, S., Mouchot, N., Ruiz, G., & Guillocheau, F. (2011). Late Triassic–early Jurassic block tilting along E–W faults, in southern Tunisia: New interpretation of the Tebaga of Medenine. *Journal of African Earth Sciences*, 61(1), 94–104. <https://doi.org/10.1016/j.jafrearsci.2011.05.007>
- Said, A., Baby, P., Chardon, D., & Ouali, J. (2011). Structure, paleogeographic inheritance, and deformation history of the southern Atlas foreland fold and thrust belt of Tunisia. *Tectonics*, 30(6), TC6004. <https://doi.org/10.1029/2011tc002862>
- Scotese, C. R., & Schettino, A. (2017). Chapter 3 - late permian-early Jurassic paleogeography of western Tethys and the world. In J. I. Soto, J. F. Flinch, & G. Tari (Eds.), *Permo-triassic salt provinces of Europe, North Africa and the Atlantic margins* (pp. 57–95). Elsevier.
- Simancas, J. F., Tahiri, A., Azor, A., Lodeiro, F. G., Martínez Poyatos, D. J., & El Hadi, H. (2005). The tectonic frame of the Variscan–Alleghanian orogen in southern Europe and northern Africa. *Tectonophysics*, 398(3), 181–198. <https://doi.org/10.1016/j.tecto.2005.02.006>
- Soua, M. (2013). First evidence of tunnel valley-like formation during the late ordovician "subglacial" period in southern Tunisia. In *Influence on the Jeffara sandstone reservoir quality, paper presented at SPE Middle East oil and gas show and conference*. Manama.
- Soua, M. (2014). Paleozoic oil/gas shale reservoirs in southern Tunisia: An overview. *Journal of African Earth Sciences*, 100, 450–492. <https://doi.org/10.1016/j.jafrearsci.2014.07.009>
- Soussi, M., Niedźwiedzki, G., Talanda, M., Drózd, D., Sulej, T., Boukhalfa, K., et al. (2017). Middle Triassic (Anisian-Ladinian) Tejra red beds and Late Triassic (Carnian) carbonate sedimentary records of southern Tunisia, Saharan Platform: Biostratigraphy, sedimentology and implication on regional stratigraphic correlations. *Marine and Petroleum Geology*, 79, 222–256. <https://doi.org/10.1016/j.marpetgeo.2016.10.019>
- Stampfli, G. M., & Borel, G. D. (2002). A plate tectonic model for the Paleozoic and Mesozoic constrained by dynamic plate boundaries and restored synthetic oceanic isochrons. *Earth and Planetary Science Letters*, 196(1), 17–33. [https://doi.org/10.1016/s0012-821x\(01\)00588-x](https://doi.org/10.1016/s0012-821x(01)00588-x)
- Troudi, H., Chevalier, F., Alouani, W., Mzoughi, W., & Abdelkader, O. (2018). Insight on the exploration potential of the ordovician gas play in Tunisia Ghadames Basin, North Africa. In *Paper presented at Abu Dhabi International petroleum exhibition & conference Abu Dhabi, UAE*.
- Wolfe, M. R., & Stockli, D. F. (2010). Zircon (U–Th)/He thermochronometry in the KTB drill hole, Germany, and its implications for bulk He diffusion kinetics in zircon. *Earth and Planetary Science Letters*, 295(1), 69–82. <https://doi.org/10.1016/j.epsl.2010.03.025>
- Zaafouri, A., Haddad, S., & Mannai-Tayech, B. (2017). Subsurface Permian reef complexes of southern Tunisia: Shelf carbonate setting and paleogeographic implications [Dataset]. *Journal of African Earth Sciences*, 129, 944–959. <https://doi.org/10.1016/j.jafrearsci.2017.02.032>